Convergence analysis and applicability of a domain decomposition method with nonlocal interface boundary conditions

Hongru Li[a,*], Miltiadis V. Papalexandris[a]

[a] *Institute of Mechanics, Materials and Civil Engineering, Université catholique de Louvain, Place du Levant 2, Louvain-la-Neuve, 1348, Belgium.*

Abstract

In the past, the domain decomposition method was developed successfully for solving large-scale linear systems. However, the problems with significant nonlocal effect remain a major challenger for applying the method efficiently. In order to sort out the problem, a non-overlapping domain decomposition method with nonlocal interface boundary conditions was recently proposed and studied both theoretically and numerically. This paper is the report on the further development of the method, aiming to provide a comprehensive convergence analysis of the method, with supplementary numerical tests to support the theoretical result. The nonlocal effect of the problem is found to be reflected in both the governing equation and boundary conditions, and the effect of the latter was never taken into account, although playing a significant role in affecting the convergence. In addition, the paper extends the applicability of the analysis result drawn from the Poisson's equation to more complicated problems by examining the symbols of the Steklov-Poincaré operators. The extended application includes a model equation arising from fluid dynamics and the high performance of the domain decomposition method in solving this equation is better elaborated.

Keywords: Fourier analysis, parallel computing, Poisson's equation, separation of variables, Steklov-Poincaré operators, domain decomposition method

1. Introduction

The method of domain decomposition (DD) has been proven efficient in resolving both nonlocal model problems [1–3] and large-scale linear systems arising in various scientific and engineering applications, including those involving the identification of data on the boundary, known as Cauchy inverse problems [4, 5]. Meanwhile, the rapid development of the parallel computing technology calls for smarter DD algorithm design to achieve a more efficient distributed of the workload among subdomains and data exchange on the interfaces. The DD method partitions the entire computational domain into multiple subdomains. Correspondingly, the global problem is decomposed into various local problems and assigned to different CPU cores to solve them independently. The continuity of the local solutions among different subdomains depends entirely on the data exchange rules on the interfaces, which formulate the so-called interface boundary conditions (IBCs). Over the years, there has been a significant number of approaches for developing DD schemes of various kinds, and this paper particularly considers the non-overlapping partition with the exact transmission IBCs.

In the non-overlapping DD method, the appropriate construction of the IBCs plays a crucial role in ensuring the solution's global continuity and improving the convergence of the entire method. The general goal for designing an efficient DD method is to construct the most exact IBCs to minimise the global iterations. To achieve this, one may formulate the exact IBC by evaluating the surface potentials [6, 7]. Alternatively, another popular scheme is to apply the nonlocal Dirichlet-to-Neumann (DtN) map on the interface boundary. The DtN map essentially consists of the analytical

*Corresponding author
Email address: hongru.li@uclouvain.be (Hongru Li)

relations to ensure the continuity of both the function and its derivatives between two adjacent subdomains. Mathematically, this dual continuity is represented by Steklov-Poincaré (SP) operators in the analytical relations. The DtN map has been proven effective in capturing the nonlocal effect of the function at the interface, thus allowing for the non-iterative convergence on the global scale [8]. In practice, the implementation of the DtN map usually results in the Robin-Robin IBCs because of this dual continuity. Interestingly, the resulting method with the Robin-Robin IBCs (henceforth referred to as the Robin-Robin method) could be considered as the optimised Schwartz method due to the aforementioned non-iterative property of the DtN map. Various Robin-Robin methods are developed and applied to improve the computational efficiency [9, 10] and designing preconditioner [11, 12]. In particular, the convergence of the Robin-Robin method has been studied extensively for non-linear elliptic equations with a p-structure [13] and time-dependent parabolic equations [14].

Since the nonlocal DtN map calculation involves the unknown function on the interface, this map cannot be applied in a straightforward manner. One common remedy is to use the value of the function from the last iteration. However, in this manner the non-iterative property is lost due to incurring global iterations. Such is the case in [15] for solving a Helmholtz equation in an unbounded domain. Apart from this idea, one may approximate the SP operators with acceptable computational cost; otherwise, the approximation cost could be higher than the savings of applying the DtN map. One approach for approximating the SP operators is to apply spectral expansion on them. The expansion results in a set of eigenvalue problems to solve, and the SP operators are approximated by considering the truncated eigenfunction basis set [16]. The approximation may also be realised by radial basis function interpolation [17]. Besides, it is noted that much of the approximation is considered in the context of discrete form, for example, boundary concentrated finite element method [18], finite element tearing and interconnecting method [12], finite element method [19] as well as finite element method particularly for Stokes equation [20] and hybrid finite element method particularly for the Poisson's equation [21]. Clearly, the approximation schemes are all dependent on the numerical scheme and the problem itself.

In [22], a non-overlapping domain decomposition method with nonlocal IBCs was proposed. Therein the nonlocal IBCs were constructed by applying the SP operators on Taylor interface function expansions and making approximations in geometric order: constant, linear and quadratic ones. Accordingly, three algorithms were derived. Also, the convergence analysis of the method for the Poisson's equation was performed via the Fourier method, also applied in [23]. The Poisson's equation was chosen not only because it is convenient for deriving analytical results [8, 17], but also because it is widely encountered in engineering applications such as the pressure solver in fluid dynamics [24]. Then, the numerical test on a two-dimensional model equation in [22] (also studied in [7]) demonstrated its promising potential to be applied in wall-bounded viscous flow modelling, as opposed to the conventional nonlocal DD methods with Robin-Robin IBCs, including the so-called optimised Schwarz method. Readers who are interested in the development of the (modified and optimised) Schwarz method are encouraged to refer to Section 2.2 of [22] or the relevant work [25–28].

The convergence of the proposed domain decomposition method by [22] is analytically studied with respect to Poisson's equation, and the superior efficiency of the method in application to resolving wall-bounded flow is demonstrated by numerical tests. Despite the successful efforts, several issues remain open and require further analysis. These are the following:

1. The convergence rate calculation was only performed for the algorithm with the constant approximation of the SP operators. The calculation for the other two algorithms should be performed to make a complete theoretical analysis of the entire method.
2. The SP operator was simplified to one dimension when performing the convergence rate calculation (we denote the method by standard approach). Nevertheless, this approach could incur an unacceptable error for the problems with strong nonlocal effect. The result of the standard approach excludes the boundary effect, thus not being fully capable of matching the result of the numerical test where the boundary effect is incorporated.

3. The convergence analysis was based on the Poisson's equation but was not associated with the model equation to which the method is aimed to be applied.

The present paper aims at addressing these issues. More specifically, we perform herein further convergence analysis of the DD method and repeat the numerical tests reported in [22]. Subsequently, we extend the convergence analysis to all the three algorithms without making simplified assumptions about the SP operators. Furthermore, additional numerical tests are performed herein to verify the theoretical analysis and help provide a clearer understanding of how the DD method captures the nonlocal effect of the problem. Naturally, the present paper inherit some of the essential approaches/notations and numerical results of [22] as the foundation of the current work, so as to maintain consistent standard of the study between the two papers. With the key information well preserved, the inherited approaches/notation/result might only be briefly elaborated again to avoid redundancy. The overarching objective of the paper is to make a more comprehensive convergence analysis of the method based on the Poisson's equation and cast more light on the extensive applicability of the method to more complex problems.

This paper is organised as follows. Section 2 performs the convergence rate calculation for all the three algorithms, presuming dropping the boundary effect (so-called standard approach). In Section 3, the convergence rate calculation result of the algorithms is analysed and developed into corresponding methods to evaluate the convergence rate. The evaluation methods depend only on the symbols of the SP operators associated with the given problem, so they are easy to implement and, more importantly, are able to make general sense for a class of problems. In Section 4, the influence of the boundary effect on the convergence is considered. In Section 5, the numerical tests are carried out to verify the convergence analysis result with both the standard approach conditions and the boundary effect. Finally, Section 6 concludes.

2. Convergence rate calculation

This section performs the (standard) convergence rate calculation of the domain decomposition method as proposed in [22]. First, we outline this method.

Consider a boundary value problem (BVP) in the domain $\Omega \subset \mathbb{R}^2$, where $\mathcal{L}$ is an elliptic operator.

$$\begin{aligned} &\mathcal{L}u = f, \\ &u = g \quad \text{on } \partial\Omega. \end{aligned} \tag{1}$$

The domain is decomposed into two subdomains: $\Omega = \Omega_1 \cup \Omega_2$ by the interface $\Gamma := \partial\Omega_1 \cap \partial\Omega_2$. Then the two BVPs are formulated respectively:

$$\begin{aligned} \mathcal{L}u_i = f_i,\ (i = 1, 2) \\ u_i = g_i \quad \text{on } \partial\Omega_i \setminus \Gamma, \\ u_{1y}^{n+1} + S_2[u_1^{n+1}] = u_{2y}^{n} + S_2[u_2^{n}] \quad \text{on } \Gamma, \\ -u_{2y}^{n+1} + S_1[u_2^{n+1}] = -u_{1y}^{n} + S_1[u_1^{n}] \quad \text{on } \Gamma, \end{aligned} \tag{2}$$

where S_i stands for the SP operators [29].

As mentioned earlier, Eq.(2) is not easy to implement directly because the computational cost of obtaining the SP operators is formidably high. To realize a simpler implementation of the method, the SP operators need to be approximated: they are applied to the local Taylor expansion of the function on the interface. The domain decomposition method we consider in this paper is derived on the basis of the above approximation. Depending on the expansion order, there are three algorithms developed from the method, namely RR-SP0, RR-SP1 and RR-SP2 respectively. The algorithms differ from one another in the formulation of the IBCs, as will be shown in the rest part of this section.

2.1. RR-SP0: Separation of variables

In this subsection, we briefly review the convergence rate calculation of RR-SP0 (algorithm with constant approximation of the SP operators) applied to the Poisson's equation. The calculation was performed in the framework of separation of variables, as shown in Section 3 and Appendix A of [22].

The calculation was performed with respect to the Poisson's equation:

$$-\nabla^2 u = f. \tag{3}$$

The domain is rectangular, $\Omega : \{0 < x < L,\ 0 < y < B\}$. The interface Γ is at $y^* = A$ $(0 < A < B)$.

In RR-SP0, the interface boundary conditions at y^* read:

$$\begin{aligned} u_{1y}^{n+1} + S_2[I]u_1^{n+1} &= u_{2y}^n + S_2[I]u_2^n, \\ -u_{2y}^{n+1} + S_1[I]u_2^{n+1} &= -u_{1y}^n + S_1[I]u_1^n. \end{aligned} \tag{4}$$

The unit function $I(x) = 1$ is defined in the entire domain. Importantly, it was assumed that $S_i[I]$ $(i = 1, 2)$ is constant: $S_1[I] \equiv S_1^*[I] = 1/A$, $S_2[I] \equiv S_2^*[I] = 1/(B - A)$ for the convenience of performing convergence analysis. Strictly speaking, this assumption is not true for functions defined in bounded domain, especially at the vicinity of the boundaries, for example, see Fig.8, where the red line represents the simplified profile (constant) of $S_i[I]$ and the blue line is the actual profile. The notation $S_i^*[I]$ represents the constant version of $S_i[I]$ (which is not a constant as shown), and they are considered to be equal at the moment.

The error problem ($e^n := u - u^a$, where u^a is the approximated solution) is governed by a Laplace's equation with the homogeneous boundary conditions at $\partial\Omega \cap \partial\Omega_i$ $(i = 1, 2)$ for each subdomain. The IBCs for the error problem at interface Γ are:

$$\begin{aligned} e_{1y}^{n+1} + S_2^*[I]e_1^{n+1} &= e_{2y}^n + S_2^*[I]e_2^n, \\ -e_{2y}^{n+1} + S_1^*[I]e_2^{n+1} &= -e_{1y}^n + S_1^*[I]e_1^n. \end{aligned} \tag{5}$$

We apply separation of variables to solve the Laplace's equation. We assume that the solution has the form: $e_i^n(x, y) := b_i(x)\hat{e}_i^n(y)$. It is actually shown that $b_i(x) = \sin(\frac{k\pi x}{L})$ corresponds to the eigenfunction of the SP operators [22]. The iterative relation between the two subdomains is given by the eigenvalues of the SP operators that correspond to the eigenfunction $b_i(x)$:

$$\|\hat{e}_{i|\Gamma}^{n+1}\| = \left| \frac{\frac{1}{A} - \frac{k\pi}{L}\coth(\frac{k\pi A}{L})}{\frac{1}{A} + \frac{k\pi}{L}\coth(\frac{k\pi(B-A)}{L})} \cdot \frac{\frac{1}{B-A} - \frac{k\pi}{L}\coth(\frac{k\pi(B-A)}{L})}{\frac{1}{B-A} + \frac{k\pi}{L}\coth(\frac{k\pi A}{L})} \right| \|\hat{e}_{i|\Gamma}^{n-1}\|. \tag{6}$$

$$(k = 1, 2, ...)$$

It is noted that the eigenvalues for SP1 and SP2 operators are $\lambda_1 = \frac{k\pi}{L}\coth\frac{k\pi A}{L}$ and $\lambda_2 = \frac{k\pi}{L}\coth\frac{k\pi(B-A)}{L}$ respectively.

2.2. RR-SP0: Fourier transform

In this subsection, we perform the convergence rate calculation of RR-SP0 by means of Fourier transform. The two methods are quite similar and the calculation result is fully consistent with that from separation of variables. The two methods differ in the treatment of the SP operators, but these treatments yield the same result. The treatment in Fourier transform will be used in Subsection 2.4 for the convergence rate calculation for RR-SP1 and RR-SP2.

We consider the same error problem (the Laplace's equation) as well as the IBCs. First we apply the Fourier transform to the error equations in the two subdomains with respect to (w.r.t.) y and consider the two homogeneous boundary conditions. The solution w.r.t. x is given:

$$\hat{e}_i(\omega, x) = \sin(\omega x). \quad \omega = \frac{k\pi}{L},\ k = 1, 2, ... \tag{7}$$

The calculation result constrains the value of ω to be discontinuous.

Next, we apply the Fourier transform in the equations in the two subdomains w.r.t. x. It yields two ordinary differential equations (ODEs):

$$\hat{e}_{iyy}^{n+1}(\omega, y) - \omega^2 \hat{e}_i^{n+1}(\omega, y) = 0. \quad (i = 1, 2) \tag{8}$$

The boundary conditions for the two problems are:

$$\begin{cases} \hat{e}_1^{n+1}(0) = 0, \\ \hat{e}_{1y}^{n+1}(A) + \frac{1}{2\pi}\mathcal{F}(S_2[I]) * \hat{e}_1^{n+1}(A) = -\hat{e}_{2y}^{n}(A) + \frac{1}{2\pi}\mathcal{F}(S_2[I]) * \hat{e}_2^{n}(A). \end{cases} \tag{9}$$

$$\begin{cases} \hat{e}_2^{n+1}(\omega, 0) = 0, \\ -\hat{e}_{2y}^{n+1}(A') + \frac{1}{2\pi}\mathcal{F}(S_1[I]) * \hat{e}_2^{n+1}(A') = -\hat{e}_{1y}^{n}(A') + \frac{1}{2\pi}\mathcal{F}(S_1[I]) * \hat{e}_1^{n}(A'). \end{cases} \tag{10}$$

It is noted that $A' = A - B$. In addition, the sign '*' denotes convolution calculation. To simplify the convolution, it is assumed that the unit function I is defined in the real domain $\mathbb{R}$ rather than $[0, L]$. As a result, the following convolution term is readily obtained:

$$\frac{1}{2\pi}\mathcal{F}(S_i[I]) * \hat{e}_j = \frac{1}{2\pi}\int_{-\infty}^{\infty} \hat{S}_i(\tau) 2\pi\delta(\tau)\hat{e}_j(\omega - \tau)d\tau = \hat{S}_i(0)\hat{e}_j(\omega). \tag{11}$$

The symbol of the pseudo-operator S_i is denoted by $\hat{S}_i(\omega)$. The Fourier transform of I yields $2\pi\delta$, where δ is the Dirac delta function. Due to the sifting property of the Dirac delta function, only one wave number regarding $\hat{S}_i$ needs to be considered, $\omega = 0$, which largely simplifies the calculation. It is clear that the integration containing δ should be considered within the scope of generalized function (distribution), rather than classic integral of conventional functions.

The solution to the ODEs (8) is:

$$\hat{e}_1^{n+1}(k, A) = \frac{\omega \coth(\omega(A - B)) + \hat{S}_2(0)}{\omega \coth(\omega A) + \hat{S}_2(0)} \hat{e}_2^{n}(\omega, A), \tag{12}$$

$$\hat{e}_2^{n+1}(\omega, A) = \frac{-\omega \coth(\omega A) + \hat{S}_1(0)}{-\omega \coth(A - B) + \hat{S}_1(0)} \hat{e}_1^{n}(\omega, A). \tag{13}$$

The symbols of S_1 and S_2 are obtained as (see Appendix A):

$$\hat{S}_1(\omega) = \omega \coth(\omega A), \quad \hat{S}_2(\omega) = \omega \coth(\omega(B - A)). \tag{14}$$

Therefore, $\hat{S}_1(0) = 1/A$, and $\hat{S}_2(0) = 1/(B - A)$. We substitute them into Eqs.(12) and (13), and consider the value of ω as shown in Eq.(7), the convergence rate is obtained and it is equal to that obtained from separation of variables, see Eq.(6).

2.3. Standard approach and generalized convergence rate calculation

In the previous subsections, the convergence rate calculation was performed by both separation of variables and Fourier transform. On one hand, the Fourier transform solves the problem by solving two one-dimensional BVPs independently in the framework of separation of variables. On the other hand, the two approaches differ technically in the treatment of $S_i[I]$: the separation of variables assumes $S_i[I]$ is constant, and the Fourier transform assumes I is defined in $\mathbb{R}$. The two approaches lead to equal convergence rate as a result of they both considering only the zero wave number harmonic in Fourier space. In practical case (rather than the ideal case where the assumptions are made) the domain of the unit function is constrained, for example, I is defined in $[0, L]$, and we denote the constrained function by I'. To obtain fully accurate convergence rate, the Fourier transform should have been applied to I' :

$$\hat{I}' := \mathcal{F}[I'] = \frac{1}{\omega}\sin(\omega L) + j\frac{\cos(\omega L) - 1}{\omega}. \tag{15}$$

It is noted that j is the imaginary unit. The energy spectrum of $\hat{I}'$ is illustrated in Fig.1 (upper left) with $L = 1$. As it can be seen, the Fourier transform is no longer dominated only by the zero wave number harmonic but it is also influenced by other wave number harmonics. The main energy is distributed in the small wave number band, which become increasingly narrower as L becomes larger. The peak value becomes higher with larger L. In the case $L \to \infty$ (in both directions), all energy is concentrated in $\omega = 0$ and $\mathcal{F}[I']$ becomes the Dirac delta function.

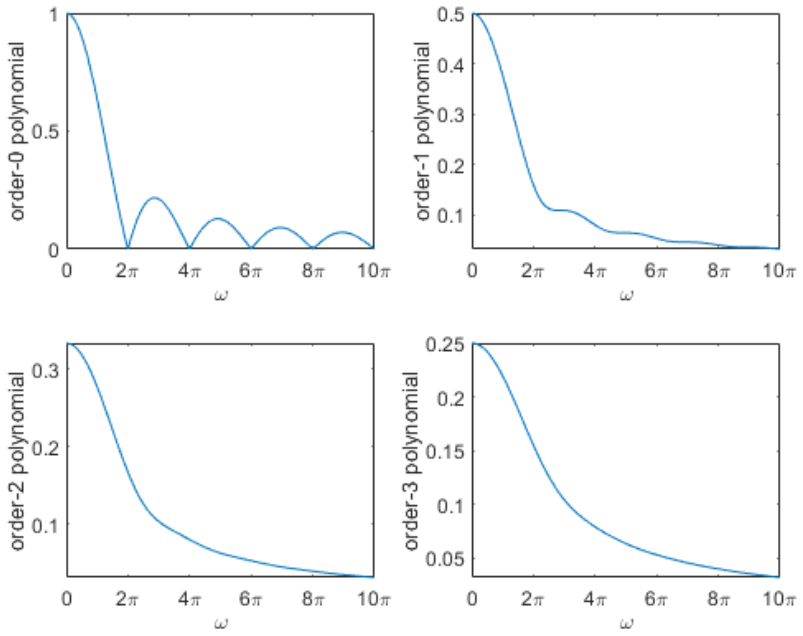


Figure 1: The energy spectrum of polynomials I, x, x^2 and x^3 defined in $[0, 1]$.

In the case of the domain of I being constrained, $S_i[I']$ could be obtained by considering the inverse Fourier transform of $\hat{S}_i[\hat{I}']$:

$$S_i I := \mathcal{F}^{-1}[\hat{S}_i[\hat{I}']] = \frac{1}{2\pi}\int_{-\infty}^{\infty} \hat{S}_i(\omega) I' e^{j\omega x} d\omega. \tag{16}$$

The expressions of $\hat{S}_i$ and $\hat{I}'$ are given in Eq.(14) and Eq.(15) respectively. The inverse transform would yield a complex function. However, if the function is defined in the entire real domain so that only the zero wave number is considered, and $\hat{I}'$ becomes 2π times the Dirac Delta function:

$$\frac{1}{2\pi}\int_{-\infty}^{\infty} \hat{S}_i(\omega) I' e^{j\omega x} d\omega = \frac{1}{2\pi}\int_{-\infty}^{\infty} \hat{S}_i(\omega) 2\pi\delta(\omega) d\omega = \hat{S}_i(0). \tag{17}$$

It shows that $S_i[I]$ is a constant, which is exactly the assumption made by separation of variables. This analysis shows that despite the different technical treatments, the two approaches are essentially equal and amount to considering only the zero wave number term in Fourier space. The condition to exclude non-zero wave numbers is that the boundaries w.r.t. x are unbounded ($x \in \mathbb{R}$). Therefore, the approach that considers only the zero wave number (standard approach) could also be interpreted as the 'boundary-effect-free' approach. Next in Subsection 2.4, the standard approach would be applied to the convergence rate calculation of RR-SP1 and RR-SP2 via Fourier transform. In those calculations, $S_i[x]$ and $S_i[x^2]$ are treated the same way as $S_i[I]$: assume no boundary effect by setting $x \to \pm\infty$. Clearly, assuming $x \to \pm\infty$ is much easier than presuming the simplified profile of $S_i[x]$ and $S_i[x^2]$. Therefore, the Fourier transform is more convenient to implement than the separation of variables.

It is seen in Eq.(6) that each single term corresponds to a symbol of the SP operators. The result could be applied to all BVPs that have variable-separation form. Next we consider a general error

problem as proof:

$$\mathcal{L}e_i^{n+1} = 0. \tag{18}$$

The linear operator $\mathcal{L}$ is not known. The BVP is defined in the same square domain Ω: $\{0 < x < L,\, 0 < y < B\}$, with interface boundary at $y^* = A\,(0 < A < B)$. The IBCs are of RR-SP0 type, see Eq.(5).

We apply Fourier transform w.r.t. x on the BVP and one obtains the one-dimensional problem about $\hat{e}_i^{n+1}(\omega, y)$. Apply the IBCs:

$$\hat{e}_{1y}^{n+1}(\omega, A) + \hat{S}_2(0)\hat{e}_1^{n+1}(\omega, A) = \hat{e}_{2y}^{n}(\omega, A) + \hat{S}_2(0)\hat{e}_2^{n}(\omega, A) \tag{19}$$

$$-\hat{e}_{2y}^{n+1}(\omega, A) + \hat{S}_1(0)\hat{e}_2^{n+1}(\omega, A) = -\hat{e}_{1y}^{n}(\omega, A) + \hat{S}_1(0)\hat{e}_1^{n}(\omega, A). \tag{20}$$

Let us rearrange:

$$\hat{e}_1^{n+1}(\omega, A) = \frac{\hat{e}_{2y}^{n}(\omega, A) + \hat{S}_2(0)\hat{e}_2^{n}(\omega, A)}{\kappa_1^{n+1}(\omega, A) + \hat{S}_2(0)}, \tag{21}$$

$$\hat{e}_2^{n+1}(\omega, A) = \frac{-\hat{e}_{1y}^{n}(\omega, A) + \hat{S}_1(0)\hat{e}_1^{n}(\omega, A)}{-\kappa_2^{n+1}(\omega, A) + \hat{S}_1(0)}, \tag{22}$$

where $\kappa_i^{n+1}(\omega, A) := \hat{e}_{iy}^{n+1}(\omega, A)/\hat{e}_i^{n+1}(\omega, A)$. The formula to calculate κ_i^n almost coincide with the eigenvalue calculation of the SP operators (see the appendix of [22]), and κ_i is actually independent from iteration step n:

$$\kappa_1^{n+1} := \frac{\hat{e}_{1y}^{n+1}(\omega, A)}{\hat{e}_1^{n+1}(\omega, A)} = \lambda_1(\omega), \quad \kappa_2^{n+1} := \frac{\hat{e}_{2y}^{n+1}(\omega, A)}{\hat{e}_2^{n+1}(\omega, A)} = -\lambda_2(\omega). \tag{23}$$

On the other hand, the definition of the eigenvalue gives:

$$\lambda_i(\omega) := \frac{\mathcal{F}[S_i[e_1(x, A)]]}{\mathcal{F}[e_1(x, A)]} = \frac{\hat{S}_i(\omega)\hat{e}_1(\omega, A)}{\hat{e}_1(\omega, A)} = \hat{S}_i(\omega). \tag{24}$$

Therefore, the eigenvalues of the SP operators are equal to the symbols of the SP operators. The iterative relationship, Eqs.(21) and (22), between $\hat{e}_i^{n+1}$ and $\hat{e}_j^{n}$ ($i \neq$j) is transformed by substituting κ_1 with $\hat{S}_1$ and κ_2 with $-\hat{S}_2$:

$$\hat{e}_1^{n+1}(\omega, A) = \frac{-\hat{S}_2(\omega) + \hat{S}_2(0)}{\hat{S}_1(\omega) + \hat{S}_2(0)}\hat{e}_2^{n}(\omega, A), \tag{25}$$

$$\hat{e}_2^{n+1}(\omega, A) = \frac{-\hat{S}_1(\omega) + \hat{S}_1(0)}{\hat{S}_2(\omega) + \hat{S}_1(0)}\hat{e}_1^{n}(\omega, A). \tag{26}$$

The convergence rate is then obtained directly:

$$\|\hat{e}_i^{n+1}\| = \left|\frac{\hat{S}_1(0) - \hat{S}_1(\omega)}{\hat{S}_1(0) + \hat{S}_2(\omega)} \cdot \frac{\hat{S}_2(0) - \hat{S}_2(\omega)}{\hat{S}_2(0) + \hat{S}_1(\omega)}\right| \|\hat{e}_i^{n-1}\|. \tag{27}$$

This is the generalized convergence rate of RR-SP0 for BVPs that could be solved via separation of variables. Clearly, the symbols of the SP operators associated with the given problem determine the convergence of RR-SP0. In the Poisson's equation, the result is shown in Eq.(6).

In the general case, the symbols are not only functions of ω, but also of x. This in turn implies that it is harder to solve for the symbols. However, the convergence rate can still be expressed by Eq.(27) since there is no assumption made with the derivation of Eq.(27).

2.4. RR-SP1 and RR-SP2

In this subsection, we consider the same Poisson's equation and perform the convergence rate calculation of RR-SP1 and RR-SP2 via Fourier transform. The same assumption is made as above, i.e., the function is defined in an infinite domain ($x \in \mathbb{R}$) when addressing $S_i[x]$ and $S_i[x^2]$.

Consider the Poisson's equation defined in the same domain with interface $y^* = A$. For the error problem, the IBCs of RR-SP1 read:

$$\begin{aligned} e_{1y}^{n+1} + S_2[I]e_1^{n+1} + T_{1l}e_{1x}^{n+1} &= e_{2y}^n + S_2[I]e_2^n + T_{1l}e_{2x}^n, \\ -e_{2y}^{n+1} + S_1[I]e_2^{n+1} + T_{2l}e_{2x}^{n+1} &= -e_{1y}^n + S_1[I]e_1^n + T_{2l}e_{1x}^n, \end{aligned} \tag{28}$$

where $T_{1l} := S_2[x] - S_2[I]x$ and $T_{2l} := S_1[x] - S_1[I]x$.

Clearly the IBCs of RR-SP1 only differ from those of RR-SP0 by the additional terms containing T_{il}. Therefore, only the additional terms are treated herein. We apply the Fourier transform on the IBCs and the additional terms are calculated as follows:

$$\begin{aligned} &\mathcal{F}[(S_i[x] - S_i[I]x)e_{jx}] \\ &= \frac{j}{2\pi}\int_{-\infty}^{\infty}(\hat{S}_i(\tau)2\pi j\delta^{'}(\tau) - \hat{S}_i(0)2\pi j\delta^{'}(\tau))(\omega-\tau)\hat{e}_j(\omega-\tau)d\tau \\ &= -\int_{-\infty}^{\infty}[(\hat{S}_i(\tau) - \hat{S}_i(0))(\omega-\tau)\hat{e}_j(\omega-\tau)]\delta^{'}(\tau)d\tau \\ &= \omega\hat{S}_{i\omega}(0)\hat{e}_j(\omega). \end{aligned} \tag{29}$$

It is noted that $\hat{S}_{i\omega}$ is the derivative of $\hat{S}_i$ with respect to ω.

In the calculation of the additional term, $S_i[I]$ is assumed to be constant (equal to $\hat{S}_i(0)$ and $S_i^*[I]$), as consistent with the calculation of RR-SP0. In addition, x is assumed to be defined in $\mathbb{R}$ so that its Fourier transform is $2\pi j\delta^{'}$. Essentially, this is again the result of considering only the zero wave number harmonic of $\mathcal{F}[x]$. As we have seen already, this significantly simplifies the calculation by the virtue of the sifting property of the Dirac Delta function.

The solutions on the interface to the BVPs defined in the inner/outer subdomains are:

$$\hat{e}_1^{n+1}(\omega, A) = \frac{-\hat{S}_2(\omega) + \hat{S}_2(0) + \omega\hat{S}_{2\omega}(0)}{\hat{S}_1(\omega) + \hat{S}_2(0) + \omega\hat{S}_{2\omega}(0)}\hat{e}_2^n(\omega, A), \tag{30}$$

$$\hat{e}_2^{n+1}(\omega, A) = \frac{-\hat{S}_1(\omega) + \hat{S}_1(0) + \omega\hat{S}_{1\omega}(0)}{\hat{S}_2(\omega) + \hat{S}_1(0) + \omega\hat{S}_{1\omega}(0)}\hat{e}_1^n(\omega, A). \tag{31}$$

Upon comparison of Eqs.(25) and (26), there is only one additional term in the numerator and denominator ,respectively, that differ the result to that of RR-SP0. Then the convergence rate is obtained directly and reads:

$$\|\hat{e}_i^{n+1}\| = \left|\frac{\hat{S}_1(0) - \hat{S}_1(\omega) + \omega\hat{S}_{1\omega}(0)}{\hat{S}_1(0) + \hat{S}_2(\omega) + \omega\hat{S}_{1\omega}(0)} \cdot \frac{\hat{S}_2(0) - \hat{S}_2(\omega) + \omega\hat{S}_{2\omega}(0)}{\hat{S}_2(0) + \hat{S}_1(\omega) + \omega\hat{S}_{2\omega}(0)}\right| \|\hat{e}_i^{n-1}\|. \tag{32}$$

The value of ω should be constrained by the boundary conditions w.r.t. x: $\omega = k\pi/L$, $k = 1, 2...$, see Eq.(7).

The additional term $\omega\hat{S}_{i\omega}(0)$ is responsible for the difference of the convergence rate between RR-SP0 and RR-SP1. The analytical expressions of $\hat{S}_i$ are shown in Eq.(14), and the derivative calculation follows:

$$\begin{aligned} \hat{S}_{1\omega} &= \coth(\omega A) + A\omega(1 - \coth^2(\omega A)), \\ \hat{S}_{2\omega} &= \coth(\omega(B-A)) + (B-A)\omega(1 - \coth^2(\omega(B-A))). \end{aligned} \tag{33}$$

It is noted that $\hat{S}_{1\omega}(0) = \hat{S}_{2\omega}(0) = 0$. As a result, the convergence rate of RR-SP1 is equal to that of RR-SP0. Recall that the IBCs of RR-SP1 have only one additional term containing T_{il} that makes them different from those of RR-SP0, see Eq.(28). Now we have seen RR-SP1 is equal to RR-SP0, so T_{il} must be equal to zero (since $e_{ix} \neq 0$):

$$S_i[x] = S_i[I]x. \tag{34}$$

Since $S_i[I]$ is constant, the 'boundary-effect-free' profile of $S_i[x]$ is a linear function of x. Again, this results from the assumption that the domain of the definition of I and x is $\mathbb{R}$. The assumption will continue to be used in the convergence rate calculation of RR-SP2.

Next, we consider the convergence rate calculation of RR-SP2 on the same Poisson's equation. The IBCs of the error problem read:

$$\begin{aligned} e_{1y}^{n+1} + S_2[I]e_1^{n+1} + T_{1l}e_{1x}^{n+1} + \frac{T_{1q}e_{1xx}^{n+1}}{2} &= e_{2y}^{n} + S_2[I]e_2^{n} + T_{1l}e_{2x}^{n} + \frac{T_{1q}e_{2xx}^{n}}{2}, \\ -e_{2y}^{n+1} + S_1[I]e_2^{n+1} + T_{2l}e_{2x}^{n+1} + \frac{T_{2q}e_{2xx}^{n+1}}{2} &= -e_{1y}^{n} + S_1[I]e_1^{n} + T_{2l}e_{1x}^{n} + \frac{T_{2q}e_{1xx}^{n}}{2}, \end{aligned} \tag{35}$$

where $T_{1q} := S_2[x^2] - 2xS_2[x] + x^2S_2[I]$ and $T_{2q} := S_1[x^2] - 2xS_1[x] + x^2S_1[I]$.

The IBCs differ from those of RR-SP1 only by the additional terms containing T_{iq}. Therefore, only the addition term is treated. The Fourier transform of the term is:

$$\begin{aligned} &\mathcal{F}[(S_i[x^2] - 2xS_i[x] + x^2S_i[I])e_{jxx}] \\ =&\frac{-1}{2\pi}\mathcal{F}[S_i[x^2] - x^2\hat{S}_i(0)] * (\omega^2\hat{e}_j) \\ =&\frac{-1}{2\pi}\int_{-\infty}^{\infty}(\hat{S}_i(\tau) - \hat{S}_i(0))(-2\pi\delta^{(2)}(\tau))(\omega-\tau)^2\hat{e}_j(\omega-\tau)d\tau \\ =&\omega^2\hat{S}_{i\omega\omega}(0)\hat{e}_j(\omega). \end{aligned} \tag{36}$$

It is noted that $\hat{S}_{i\omega\omega}$ is the second order derivative of $\hat{S}_i$ with respect to ω.

In the calculation of Eq.(36), we assumed the following: a) $S_i[I]$ is constant; b) $S_i[x]$ is equal to $S_i[I]x$; c) x^2 is defined in $\mathbb{R}$. It is noted that assumption (a) has been used in both the calculation for RR-SP0 and RR-SP1, and assumption (b) is the result of assuming x is defined in $\mathbb{R}$, which has been used for the calculation of RR-SP1 as well. All the assumptions are consistently made in order to exclude all the boundary effects in all terms. Therefore, the assumptions impose exactly the same restraints on RR-SP2 as the previous calculation for RR-SP0 and RR-SP1. No overly-strict restraint is incurred. Once again, the sifting property of the Dirac delta function amounts to excluding the non-zero wave number harmonics and simplifies the calculation.

The solutions at the interface to the BVPs defined in the inner/outer subdomains are:

$$\hat{e}_1^{n+1}(\omega, A) = \frac{-\hat{S}_2(\omega) + \hat{S}_2(0) + \omega\hat{S}_{2\omega}(0) + \frac{1}{2}\omega^2\hat{S}_{2\omega\omega}(0)}{\hat{S}_1(\omega) + \hat{S}_2(0) + \omega\hat{S}_{2\omega}(0) + \frac{1}{2}\omega^2\hat{S}_{2\omega\omega}(0)}\hat{e}_2^{n}(\omega, A), \tag{37}$$

$$\hat{e}_2^{n+1}(\omega, A) = \frac{-\hat{S}_1(\omega) + \hat{S}_1(0) + \omega\hat{S}_{1\omega}(0) + \frac{1}{2}\omega^2\hat{S}_{1\omega\omega}(0)}{\hat{S}_2(\omega) + \hat{S}_1(0) + \omega\hat{S}_{1\omega}(0) + \frac{1}{2}\omega^2\hat{S}_{1\omega\omega}(0)}\hat{e}_1^{n}(\omega, A). \tag{38}$$

Compared with Eq.(30) and (31), there is only one additional term in the numerator and denominator respectively that makes the result different from that of RR-SP1. Then the convergence rate is obtained directly:

$$\begin{aligned} &\|\hat{e}_i^{n+1}\| = \\ &\left|\frac{\hat{S}_1(0) - \hat{S}_1(\omega) + \omega\hat{S}_{1\omega}(0) + \frac{1}{2}\omega^2\hat{S}_{1\omega\omega}(0)}{\hat{S}_1(0) + \hat{S}_2(\omega) + \omega\hat{S}_{1\omega}(0) + \frac{1}{2}\omega^2\hat{S}_{1\omega\omega}(0)} \cdot \frac{\hat{S}_2(0) - \hat{S}_2(\omega) + \omega\hat{S}_{2\omega}(0) + \frac{1}{2}\omega^2\hat{S}_{2\omega\omega}(0)}{\hat{S}_2(0) + \hat{S}_1(\omega) + \omega\hat{S}_{2\omega}(0) + \frac{1}{2}\omega^2\hat{S}_{2\omega\omega}(0)}\right| \|\hat{e}_i^{n-1}\|. \end{aligned} \tag{39}$$

The value of ω should be constrained by the boundary conditions w.r.t. x: $\omega = k\pi/L$, $k = 1, 2...$, see Eq.(7).

Having derived the analytical expression of $\hat{S}_i$ (see Eq.(14)), the second order derivatives could be calculated:

$$\hat{S}_{1\omega\omega}(\omega) = 2A^2\omega\coth(\omega A)(\coth^2(\omega A) - 1) + 2A(1 - \coth^2(\omega A)), \tag{40}$$

$$\begin{aligned} \hat{S}_{2\omega\omega}(\omega) =&2(B-A)^2\omega\coth(\omega(B-A))(\coth^2(\omega(B-A)) - 1) + \\ &2(B-A)(1 - \coth^2(\omega(B-A))). \end{aligned} \tag{41}$$

The value of $\hat{S}_{i\omega\omega}(0)$ is not zero, so the convergence rate of RR-SP2 differs from that of RR-SP1 and RR-SP0. Recall that the IBCs of RR-SP2 and RR-SP0 differ only by one additional term containing T_{iq}, see Eq.(35). As a result, $T_{iq} \neq 0$, which suggests that even by dropping the boundary effect, $S_i[x^2]$ is not a quadratic function of x ($S_i[x^2] \neq x^2 S_i[I]$). This result is surprising since it is already known that $S_i[x]$ is a linear function of x.

3. Convergence analysis

In this section, we analyse the analytical convergence rate result obtained in last section and develop practical methods to evaluate the convergence of the algorithms. The method requires the calculation of the SP operators only.

3.1. Convergence analysis of RR-SP0 and RR-SP1

The convergence rate of RR-SP0 is given in Eq.(27), and it could be transformed to:

$$\|\hat{e}_i^{n+1}\| = \left| 1 - \frac{\hat{S}^2(0) + \hat{S}(0)(\Delta s_1(\omega)\Delta s_2(\omega))}{\hat{S}^2(0) + \hat{S}(0)(\Delta s_1(\omega)\Delta s_2(\omega)) + \Delta s_1(\omega)\Delta s_2(\omega)} \right| \|\hat{e}_i^{n-1}\|, \tag{42}$$

where $\hat{S}(0) := \hat{S}_1(0) + \hat{S}_2(0)$, and $\Delta s_i(\omega) := \hat{S}_i(\omega) - \hat{S}_i(0)$.

Clearly, the convergence rate depends on the product of $\Delta s_1(\omega)\Delta s_2(\omega)$: the smaller this product gets, the lower (closer to zero) the convergence rate becomes. The profiles of $\hat{S}_i(\omega)$ are given in Fig.2 ($B = 1$). The figure shows that in the low-ω case, the product is negligible and the convergence rate is close to zero. When ω becomes high, $\Delta s_1(\omega)\Delta s_2(\omega) \gg \hat{S}^2(0)$, and the convergence rate is roughly equal to $1/(1+\hat{S}(0))$. Therefore, the overall convergence should be ranging between $[0, 1/(1+\hat{S}(0))]$, depending on the value of $\Delta s_1(\omega)\Delta s_2(\omega)$.

Apart from ω, the product of $\Delta s_1(\omega)\Delta s_2(\omega)$ depends on the interface boundary location A as well. In Fig.3 we illustrate the profiles of $\Delta s_1(\omega)\Delta s_2(\omega)$ for various cases of A. The figure shows that the case $A = 1/8$ corresponds to the smallest value of $\Delta s_1(\omega)\Delta s_2(\omega)$ over the entire wave number range, which suggests that the fastest convergence should occur at $A = 1/8$. Then it is followed by $A = 2/8$ and the other two cases ($A = 3/8, 4/8$) are nearly equally slow.

3.2. Convergence analysis of RR-SP2

The convergence rate of RR-SP2 is given in Eq.(39), which could be obtained analytically due to the explicitly known expression of S_i (as well as its derivatives). Nevertheless, the analytical result does not well reveal how the the convergence rate is affected by the SP operators. Similarly to the analysis with RR-SP0, in this subsection we simplify the convergence rate formula Eq.(39) and develop a practical principle to evaluate the convergence. We transform Eq.(39):

$$\begin{aligned} \|\hat{e}_i^{n+1}\| = \Bigg| & \frac{-\frac{1}{2}\omega^2 \Delta s_{1\omega\omega}(\omega^{**}) + (\frac{1}{2} - \eta_1)\omega^2 \hat{S}_{1\omega\omega}(\omega^{**})}{-\frac{1}{2}\omega^2 \Delta s_{1\omega\omega}(\omega^{**}) + (\frac{1}{2} - \eta_1)\omega^2 \hat{S}_{1\omega\omega}(\omega^{**}) + \hat{S}(\omega)} \cdot \\ & \frac{-\frac{1}{2}\omega^2 \Delta s_{2\omega\omega}(\omega^{**}) + (\frac{1}{2} - \eta_2)\omega^2 \hat{S}_{2\omega\omega}(\omega^{**})}{-\frac{1}{2}\omega^2 \Delta s_{2\omega\omega}(\omega^{**}) + (\frac{1}{2} - \eta_2)\omega^2 \hat{S}_{2\omega\omega}(\omega^{**}) + \hat{S}(\omega)} \Bigg| \|\hat{e}_i^{n-1}\|, \end{aligned} \tag{43}$$

where $\hat{S}(\omega) := \hat{S}_1(\omega) + \hat{S}_2(\omega)$ and $\Delta s_{i\omega\omega}(\omega) := \hat{S}_{i\omega\omega}(\omega) - \hat{S}_{i\omega\omega}(0)$.

The mean-value theorem is applied twice to calculate $\hat{S}_i(\omega^{**})$:

$$\hat{S}_i(\omega) - \hat{S}_i(0) = \omega \hat{S}_{i\omega}(\omega^*) = \omega(\hat{S}_{i\omega}(\omega^*) - \hat{S}_{i\omega}(0)) = \eta_i \omega^2 \hat{S}_{i\omega\omega}(\omega^{**}), \tag{44}$$

where $\omega^* = \eta_i \omega$ ($0 < \eta_i < 1$) and $0 < \omega^{**} \leq \omega^*$.

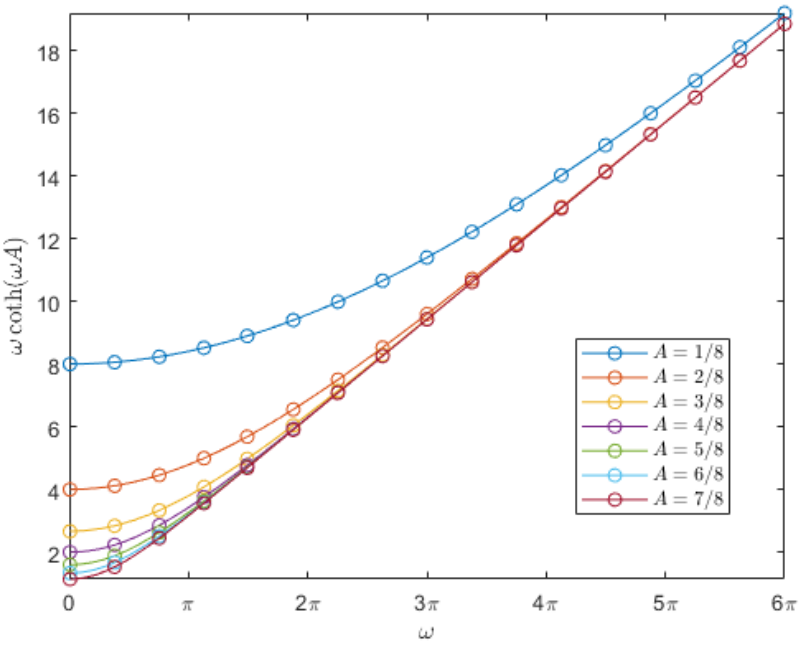


Figure 2: Profiles of $\hat{S}_1(\omega)$ with A ranging from 1/8 to 7/8. B is equal to 1. The profiles of $\hat{S}_2(\omega)$ are symmetric to those of $\hat{S}_1(\omega)$ with respect to $A = 4/8$, and are therefore not included.

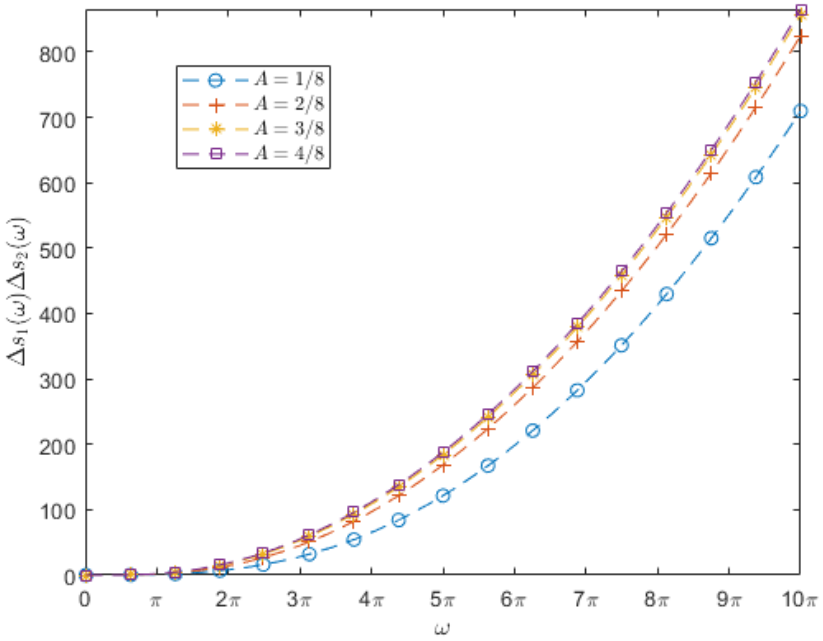


Figure 3: Profiles of $\Delta s_1 \Delta s_2$ with A ranging from 1/8 to 4/8. Since $\Delta s_1(\omega)\Delta s_2(\omega)$ is symmetric about $A = 4/8$, only four cases are plotted: $A = 1/8, 2/8, 3/8$ and $4/8$.

There are two unknown parameters (ω^{**} and η_i) yet to obtain. The parameters depend on the nature of $\hat{S}_{i\omega}$ and $\hat{S}_{i\omega\omega}$, which we choose to explore by model study. In other words, we find simple functions to model $\hat{S}_{i\omega}$ and perform the analysis on the basis of the simple functions (models).

First, it is noted that $\hat{S}_{i\omega}(\omega^*) = (\hat{S}_i(\omega) - \hat{S}_i(0))/\omega = \int_0^\omega \hat{S}_{i\omega}(Xi)dXi/\omega$. The profiles of $\hat{S}_{i\omega}(\omega)$ are plotted in Fig.4 (again $B = 1$), which shows that $\hat{S}_{i\omega}(\omega)$ is almost linear before a 'turning point' (denote ω^t) and becomes nearly flat after ω^t. Therefore, we consider a simple model to estimate $\hat{S}_{i\omega}(\omega^*)$. Here, the slope of the linear function before ω^t is denoted by l:

$$\hat{S}_{i\omega}(\omega^*) \approx \begin{cases} (\int_0^\omega l\xi d\xi)/\omega = (l\omega)/2 < l\omega^t & \omega \le \omega^t, \\ (\int_0^{\omega^t} l\xi d\xi + \int_{\omega^t}^\omega l\omega^t d\xi)/\omega = (l\omega^t(\omega - \frac{\omega^t}{2}))/\omega < l\omega^t & \omega > \omega^t. \end{cases} \tag{45}$$

The estimation shows that in either case, $\omega^* < \omega^t$. Particularly, if $\omega \gg \omega^t$, $\omega^* \approx \omega^t$. Furthermore, since $\hat{S}_{i\omega}$ is modelled as a linear function before ω^t, it could be estimated that:

$$\omega^{**} \approx \omega^*. \tag{46}$$

Second, we consider the approximation of η_i : $\eta_i \approx \hat{S}_{i\omega}(\omega^*)/(l\omega)$. The value of $\hat{S}_{i\omega}(\omega^*)$ is given in Eq.(45). If $\omega \le \omega^t$, $\eta_i \approx 1/2$. If $\omega > \omega^t$, $\eta_i \approx (l\omega^t(\omega - \frac{\omega^t}{2}))/(\omega^2) = 1/k - 1/(2k^2)$, where it is assumed that $\omega = k\omega^t$ $(k > 1)$.

If $\eta_i \approx 1/2$, the convergence rate is reduced to:

$$\|\hat{e}_i^{n+1}\| = \left| \frac{-\frac{1}{2}\omega^2 \Delta s_{1\omega\omega}(\omega^{**})}{-\frac{1}{2}\omega^2 \Delta s_{1\omega\omega}(\omega^{**}) + \hat{S}(\omega)} \cdot \frac{-\frac{1}{2}\omega^2 \Delta s_{2\omega\omega}(\omega^{**})}{-\frac{1}{2}\omega^2 \Delta s_{2\omega\omega}(\omega^{**}) + \hat{S}(\omega)} \right| \|\hat{e}_i^{n-1}\|. \tag{47}$$

If $\eta_i \approx 1/k - 1/(2k^2)$, the value of η_i depends on k. If k is close to 1, $\eta_i \approx 1/2$ and the convergence rate could still be reduced to Eq.(47). Otherwise, if $k \gg 1$, then $\omega \gg \omega^t$. As a result, $\omega^* \approx \omega^t$ as earlier mentioned, and $\omega^{**} \approx \omega^t(\omega^*)$ according to Eq.(46). In such a case, it is clear that $|\hat{S}_{i\omega\omega}(\omega^{**})| \ll |\hat{S}_{i\omega\omega}(\omega^{**}) - \hat{S}_{i\omega\omega}(0)| = |\Delta s_{i\omega\omega}(\omega^{**})|$, see Fig.5. Therefore, the term $(1/2 - \eta_i)\omega^2 \hat{S}_{i\omega\omega}(\omega^{**})$ can always be neglected, and the convergence rate can always be reduced to Eq.(47), which is equal to:

$$\|\hat{e}_i^{n+1}\| = \left| 1 - \frac{\hat{S}^2(\omega) - \frac{1}{2}\omega^2 \hat{S}(\omega) \prod_{i=1}^{i=2} \Delta s_{i\omega\omega}(\omega^{**})}{\hat{S}^2(\omega) - \frac{1}{2}\omega^2 \hat{S}(\omega) \prod_{i=1}^{i=2} \Delta s_{1\omega\omega}(\omega^{**}) + \frac{1}{4}\omega^4 \prod_{i=1}^{i=2} \Delta s_{1\omega\omega}(\omega^{**})} \right| \|\hat{e}_i^{n-1}\|. \tag{48}$$

According to this equation, the smaller the product $\prod_1^2 \Delta s_{1\omega\omega}(\omega^{**})$ gets, the smaller (close to 0) the convergence rate becomes. Meanwhile, this equation provides a practical evaluation of the convergence rate of RR-SP2 with various A. The profiles of $\prod_1^2 \Delta s_{1\omega\omega}(\omega)$ are given in Fig.6 for $B = 1$, showing that the convergence rate increases with rising A regardless of ω. Clearly the case of $A = 1/8$ should converge with the least number of iterations.

There is a simpler way to derive the transformation of Eq.(43). Recall that $\hat{S}_i(\omega) - \hat{S}_i(0) = \eta_i\omega^2 \hat{S}_{i\omega\omega}(\omega^{**})$. Then, the following approximation holds: $\hat{S}_{i\omega\omega}(\omega^{**}) \approx \hat{S}_{i\omega\omega}(0)$ because $\hat{S}_{i\omega}$ is modelled as a linear function in the considered domain: $0 < \omega^{**} < \omega^t$. The slope of the line is the same everywhere. Accordingly, Eq.(43) is transformed to:

$$\|\hat{e}_i^{n+1}\| = \left| 1 - \frac{G(\omega) + (\frac{\eta_1+\eta_2}{2} - \eta_1\eta_2)\omega^4 \prod_1^2 \hat{S}_{i\omega\omega}(0)}{G(\omega) + \frac{1}{4}\omega^4 \prod_1^2 \hat{S}_{i\omega\omega}(0)} \right| \|\hat{e}_i^{n-1}\|, \tag{49}$$

where

$$\begin{aligned} G(\omega) :=& (\hat{S}_1(0) + \hat{S}_2(\omega))(\hat{S}_2(0) + \hat{S}_1(\omega)) + \frac{\omega^2}{2}\hat{S}_{2\omega\omega}(0)(\hat{S}_1(0) + \hat{S}_2(0)) + \\ & \frac{\omega^2}{2}\hat{S}_{1\omega\omega}(0)(\hat{S}_2(0) + \hat{S}_1(0)). \end{aligned} \tag{50}$$

This suggests that the smaller the product $\prod_1^2 \hat{S}_{i\omega\omega}(0)$ gets, the smaller (close to 0) the convergence rate becomes. This simplified approach is slightly less accurate because it considers the profile

of $\hat{S}_{i\omega}$ as completely linear function before ω^t. However, this approximation method is much easier to implement since it requires the knowledge of $\hat{S}_{i\omega\omega}$ merely at $\omega = 0$ rather than over a range. The profiles of $\prod_1^2 \hat{S}_{i\omega\omega}(0)$ $(B = 1)$ are illustrated in Fig.7, showing that the case of $A = 1/8$ has the smallest convergence rate since its value of $\prod_1^2 \hat{S}_{i\omega\omega}(0)$ is the lowest. Then this case is followed by $A = 2/8, 3/8$ and $4/8$ respectively. The result completely coincides with that drawn from Fig.6, as has earlier shown.

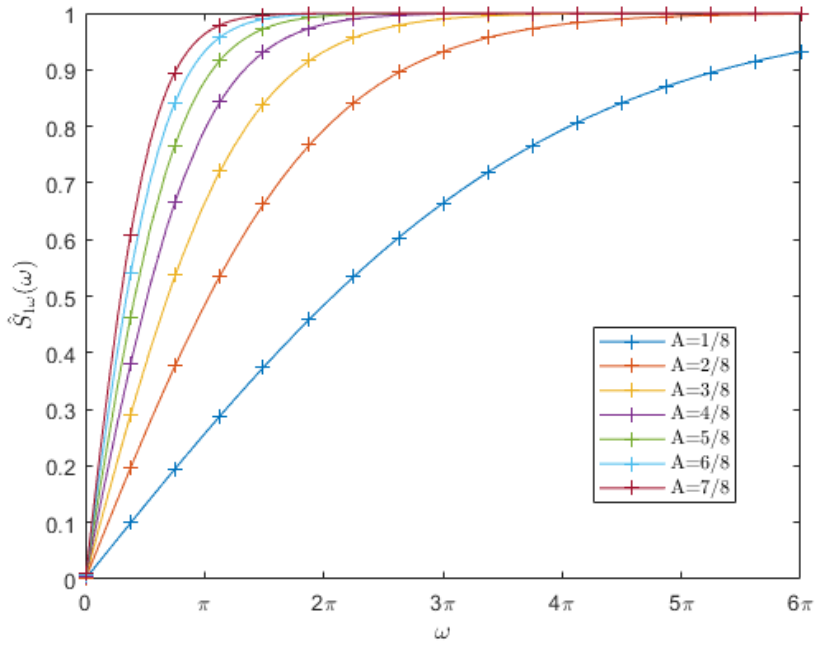


Figure 4: Profiles of $\hat{S}_{1\omega}$ with A ranging from 1/8 to 7/8. The profiles of $\hat{S}_{2\omega}$ is symmetric to those of $\hat{S}_{1\omega}$ with respect to $A = 4/8$ and are therefore not included.

4. Convergence rate calculation with the boundary effect

In this section, we perform the convergence rate calculation of RR-SP0 by taking into account the boundary effect, followed by a model study to evaluate the strength of the boundary effect. The convergence rate calculation with the boundary effect for RR-SP1 and RR-SP2 is similar to that of RR-SP0, and is also presented. It is noted that the "model study" here differs from that in Subsection 3.2 where another model is used for the convergence analysis without considering the boundary effect.

4.1. Convergence rate calculation of RR-SP0

As discussed earlier, although the exact value of $S_i[I]$ could be obtained by calculating the inverse Fourier transform of $\hat{S}_i[I']$ (so could $S_i[x]$, $S_i[x^2]$), the result is too complex to apply. For simplicity, the following model is considered:

$$S_i[I] = S_i^*[I] + P_i(x). \tag{51}$$

The first term $S_i^*[I]$ on the right stands for the result of applying the SP operators on the unit function via the standard approach (resulting in a constant), as it has been previously introduced. The second term is denoted as 'spike function' (since it looks like a spike) and represents the result of applying the SP operators to the unit function due to the boundary effect. The "spike function" could be observed from the profile of $S_i[I]$ as shown in Fig.8. The Fourier transform of $S_i[I]$ is:

$$\mathcal{F}[S_i[I]] = S_i^*[I] + \hat{P}_i(\omega). \tag{52}$$

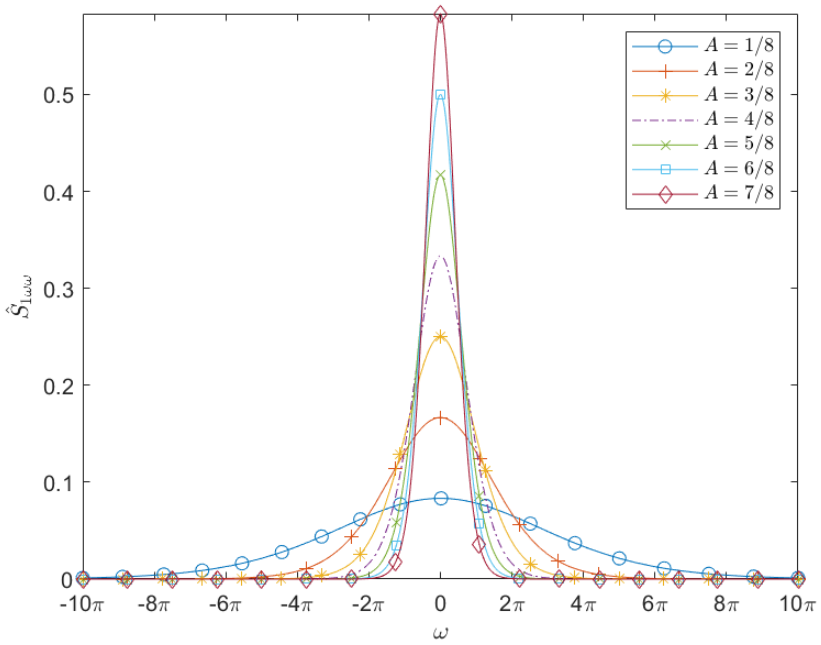


Figure 5: Profiles of $\hat{S}_{1\omega\omega}$ with A ranging from 1/8 to 7/8. The profiles of $\hat{S}_{2\omega\omega}$ are symmetric to those of $\hat{S}_{1\omega}$ with respect to $A = 4/8$ and are therefore not included.

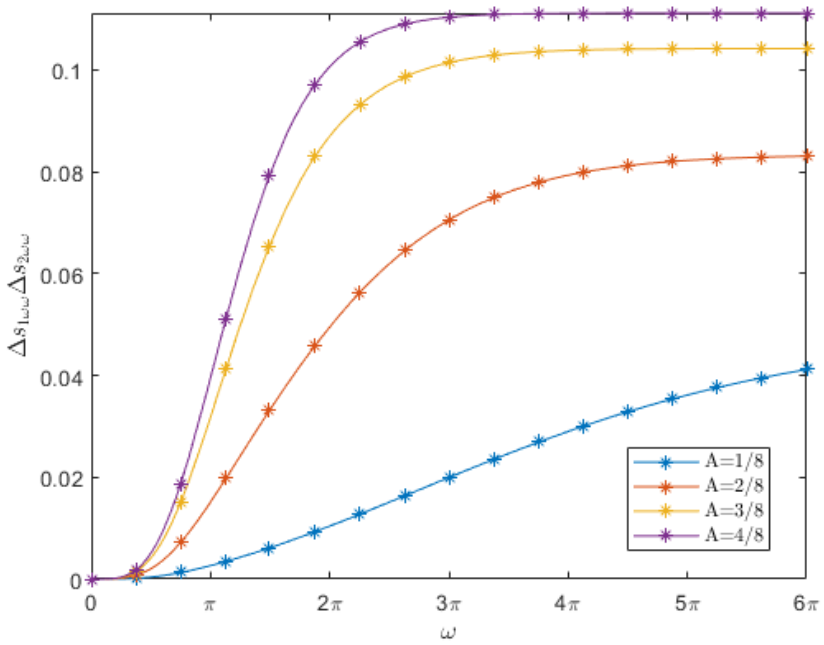


Figure 6: Profiles of $\prod_1^2 \Delta s_{1\omega\omega}(\omega^{**})$ with A ranging from 1/8 to 4/8. The profiles are symmetric with respect to $A = 4/8$ and therefore the reflection part is not plotted.

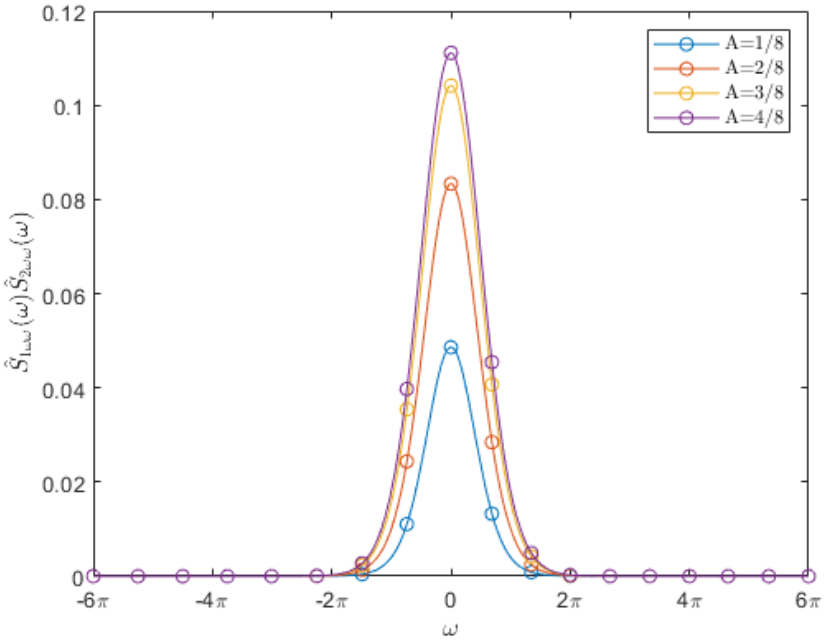


Figure 7: Profiles of $\prod_1^2 \hat{S}_{i\omega\omega}(\omega)$ with A ranging from 1/8 to 4/8. The profiles are symmetric with respect to $A = 4/8$ and therefore the reflection part is not plotted.

Next, we consider the convergence rate calculation of RR-SP0 with taking $\hat{P}_i$ accountable. For the error problem, the Fourier transform of the IBCs reads:

$$\begin{aligned} \hat{e}_{1y}^{n+1} + \hat{S}_2(0)\hat{e}_1^{n+1} + \frac{1}{2\pi}\hat{P}_2 * \hat{e}_1^{n+1} &= \hat{e}_{2y}^{n} + \hat{S}_2(0)\hat{e}_2^{n} + \frac{1}{2\pi}\hat{P}_2 * \hat{e}_2^{n}, \\ -\hat{e}_{2y}^{n+1} + \hat{S}_1(0)\hat{e}_2^{n+1} + \frac{1}{2\pi}\hat{P}_1 * \hat{e}_2^{n+1} &= -\hat{e}_{1y}^{n} + \hat{S}_1(0)\hat{e}_1^{n} + \frac{1}{2\pi}\hat{P}_1 * \hat{e}_1^{n}. \end{aligned} \tag{53}$$

The first two terms on each side of the equation are identical to those obtained with the standard approach, see Eq.(5). The third term represents the boundary effect. We recall that the iterative relationship between $\hat{e}_i^{n+1}$ and $\hat{e}_j^n$ without boundary effect is given by Eqs.(25) and (26). We denote them by $\hat{e}_1^{n+1} := \rho_1^* \hat{e}_2^n$ and $\hat{e}_2^{n+1} := \rho_2^* \hat{e}_1^n$, for example, $\rho_1^* = (-\hat{S}_2(\omega) + \hat{S}_2(0))/(\hat{S}_1(\omega) + \hat{S}_2(0))$. The overall standard convergence rate $\rho^* := \rho_1^* \rho_2^*$. If the boundary effect is considered, let us denote the convergence rate with the boundary effect by ρ (naturally $\rho := \rho_1 \rho_2$), and the boundary effect by a function $\theta_i(\omega)$:

$$\theta_i := \rho_i / \rho_i^*. \tag{54}$$

As a result, the boundary effect term (third term) on the left side of Eq.(53) is rearranged as:

$$\hat{P}_i * \hat{e}_j^{n+1} = \hat{P}_i * (\rho_j \hat{e}_i^n) := \varrho_j(\omega) \cdot (\hat{P}_i * \hat{e}_i^n). \quad i \neq j. \tag{55}$$

The yet-unknown function $\varrho_j(\omega)$ satisfies $|\varrho_j(\omega)| < 1$ because $|\hat{e}_j^{n+1}| < |\hat{e}_i^n| \Rightarrow |\hat{P}_i * \hat{e}_j^{n+1}| < |\hat{P}_i * \hat{e}_i^n|$. Let us substitute Eq.(55) into Eq.(53) and transform:

$$\frac{\hat{e}_1^{n+1}}{\hat{e}_2^n} = \frac{-\hat{S}_2(\omega) + \hat{S}_2(0)}{\hat{S}_1(\omega) + \hat{S}_2(0)} + \frac{\frac{1-\varrho_1}{2\pi}\frac{\hat{P}_2 * \hat{e}_2^n(A)}{\hat{e}_2^n(A)}}{\hat{S}_1(\omega) + \hat{S}_2(0)}, \tag{56}$$

$$\frac{\hat{e}_2^{n+1}}{\hat{e}_1^n} = \frac{-\hat{S}_1(\omega) + \hat{S}_1(0)}{\hat{S}_2(\omega) + \hat{S}_1(0)} + \frac{\frac{1-\varrho_2}{2\pi}\frac{\hat{P}_1 * \hat{e}_1^n}{\hat{e}_1^n}}{\hat{S}_2(\omega) + \hat{S}_1(0)}. \tag{57}$$

The first term on the r.h.s. stands for ρ_i^*, and the second term represents the boundary effect. Clearly, the key term to estimate the boundary effect in the above equations is:

$$(1 - \varrho_j)\frac{\hat{P}_i * \hat{e}_i^n(A)}{\hat{e}_i^n(A)}. \tag{58}$$

The calculation of the formula is case-dependent because the error function $\hat{e}_i^n$ is incorporated in the expressions.

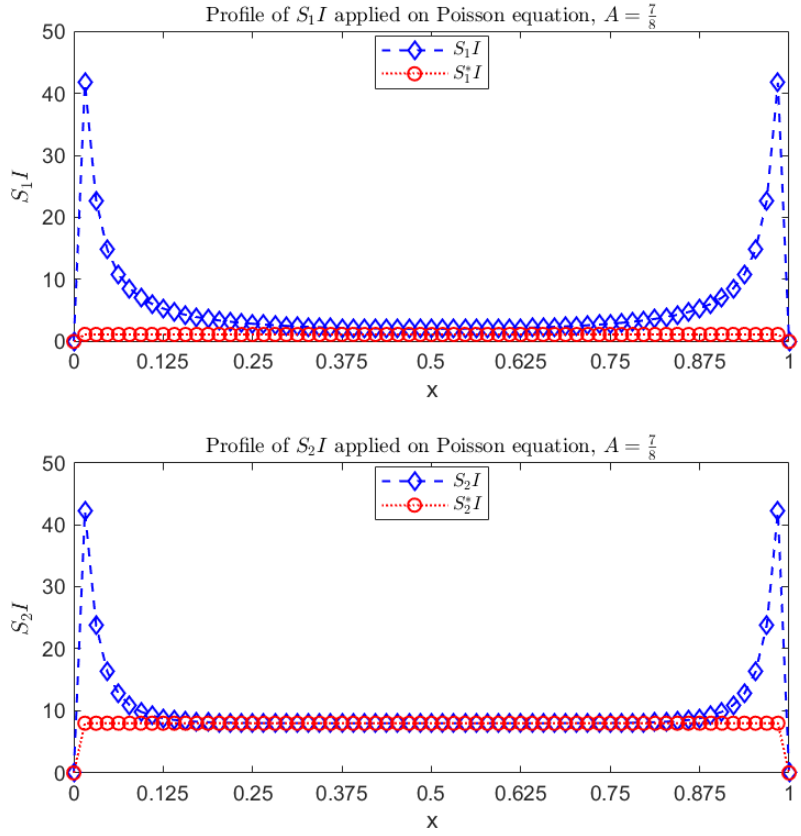


Figure 8: Profile of $S_i[I']$ applied to the Poisson's equation, $A = 7/8$. I' is defined in [0,1].

4.2. Convergence rate calculation of RR-SP1 and RR-SP2

Next, we perform the convergence rate calculation of RR-SP1 and RR-SP2 while accounting for the boundary effect.

Similarly to the approach applied to RR-SP0, $S_i[x]$ and $S_i[x^2]$ are divided by two parts:

$$S_i[x] := S_i^*[x] + P_i^l(x), \quad S_i[x^2] := S_i^*[x^2] + P_i^q(x). \tag{59}$$

The stared terms ($S_i^*[x]$ and $S_i^*[x^2]$) represent the result of applying the SP operators on x (and x^2) via the standard approach, and the second terms represent the result due to the boundary effect. Their Fourier transform are denoted by:

$$\mathcal{F}[S_i[x]] = \mathcal{F}[S_i^*[x]] + \hat{P}_i^l(\omega), \quad \mathcal{F}[S_i[x^2]] = \mathcal{F}[S_i^*[x^2]] + \hat{P}_i^q(\omega). \tag{60}$$

It is noted that in the previous calculation, $S_i[x]$ and $S_i[x^2]$ are assumed to be defined in $\mathbb{R}$ and they are not distinguished from $S_i^*[x]$ and $S_i^*[x^2]$. Since the standard approach has been extended to the approach that considers the boundary effect, the notations should differ from now on.

With the spike functions, the terms T_{il} and T_{iq} read:

$$T_{il} = (S_j^*[x] - xS_j^*[I]) + (P_j^l - xP_j) := T_{il}^* + \mathcal{P}_i^l, \ (i \neq j) \tag{61}$$

$$T_{iq} = (S_j^*[x^2] - 2x^2S_j^*[x] + x^2S_j^*[I]) + (P_j^q(x) - 2xP_j^l + x^2P_j) := T_{iq}^* + \mathcal{P}_i^q. \ (i \neq j) \tag{62}$$

We now define $T_{il}^* := S_j^*[x] - xS_j^*[I]$, $T_{iq}^* = S_j^*[x^2] - 2x^2S_j^*[x] + x^2S_j^*[I]$, $\mathcal{P}_i^l := P_j^l - xP_j$ and $\mathcal{P}_i^q := P_j^q(x) - 2xP_j^l + x^2P_j$. To maintain the notation rules consistent, in RR-SP0 case, $S_i[I]$ may be denoted by T_{ic} as well, and correspondingly $T_{ic}^* = S_i^*[I]$, $\mathcal{P}_i^c = P_i$.

Next let us consider the Fourier transform for the IBCs of the error problems. We recall that $T_{il}^* = 0$, according to Eq.(34). Then we substitute T_{il} into the IBCs of RR-SP1, see Eq.(28):

$$\hat{e}_{1y}^{n+1} + \mathcal{F}[(S_2^*[I] + P_2)e_1^{n+1}] + \mathcal{F}[\mathcal{P}_1^l e_1^{n+1}] = \hat{e}_{2y}^{n} + \mathcal{F}[(S_2^*[I] + P_2)e_2^{n}] + \mathcal{F}[\mathcal{P}_1^l e_2^{n}], \tag{63}$$

$$-\hat{e}_{2y}^{n+1} + \mathcal{F}[(S_1^*[I] + P_1)e_2^{n+1}] + \mathcal{F}[\mathcal{P}_1^l e_2^{n+1}] = -\hat{e}_{1y}^{n} + \mathcal{F}[(S_1^*[I] + P_1)e_1^{n}] + \mathcal{F}[\mathcal{P}_1^l e_1^{n}]. \tag{64}$$

Let us substitute T_{1l} and T_{iq} into the IBCs of RR-SP2, see Eq.(35):

$$\begin{aligned}\hat{e}_{1y}^{n+1} + \mathcal{F}[(S_2^*[I] + P_2)e_1^{n+1}] + \mathcal{F}[\mathcal{P}_1^l e_1^{n+1}] + \frac{1}{2}\mathcal{F}[(T_{1q}^* + \mathcal{P}_1^q)e_{1xx}^{n+1}] = \\ \hat{e}_{2y}^{n} + \mathcal{F}[(S_2^*[I] + P_2)e_2^{n}] + \mathcal{F}[\mathcal{P}_1^l e_2^{n}] + \frac{1}{2}\mathcal{F}[(T_{1q}^* + \mathcal{P}_1^1)e_{2xx}^{n}],\end{aligned} \tag{65}$$

$$\begin{aligned}-\hat{e}_{2y}^{n+1} + \mathcal{F}[(S_1^*[I] + P_1)e_2^{n+1}] + \mathcal{F}[\mathcal{P}_1^l e_2^{n+1}] + \frac{1}{2}\mathcal{F}[(T_{2q}^* + \mathcal{P}_2^q)e_{2xx}^{n+1}] = \\ -\hat{e}_{1y}^{n} + \mathcal{F}[(S_1^*[I] + P_1)e_1^{n}] + \mathcal{F}[\mathcal{P}_1^l e_1^{n}] + \frac{1}{2}\mathcal{F}[(T_{2q}^* + \mathcal{P}_2^q)e_{1xx}^{n}].\end{aligned} \tag{66}$$

Two functions $(\varrho_j^l, \varrho_j^q)$ are now introduced in an analogous manner to Eq.(55):

$$\hat{\mathcal{P}}_i^l * \hat{e}_j^{n+1} = \varrho_j^l \cdot (\hat{\mathcal{P}}_i^l * \hat{e}_i^n), \quad (i \neq j) \tag{67}$$

$$\hat{\mathcal{P}}_i^q * \hat{e}_j^{n+1} = \varrho_j^q \cdot (\hat{\mathcal{P}}_i^q * \hat{e}_i^n). \quad (i \neq j) \tag{68}$$

The (implicit) solution to the interface function in the inner/outer BVPs with RR-SP1 are:

$$\hat{e}_1^{n+1}(A) = \frac{-\hat{S}_2(\omega) + \hat{S}_2(0)}{\hat{S}_1(\omega) + \hat{S}_2(0)}\hat{e}_2^n(A) + \frac{\frac{1-\varrho_1}{2\pi}\hat{P}_2(\omega) * \hat{e}_2^n(A) + \frac{1-\varrho_1^l}{2\pi} j\mathcal{P}_2^l(\omega) * (\omega\hat{e}_2^n(A))}{\hat{S}_1(\omega) + \hat{S}_2(0)}, \tag{69}$$

$$\hat{e}_2^{n+1}(A) = \frac{-\hat{S}_1(\omega) + \hat{S}_1(0)}{\hat{S}_2(\omega) + \hat{S}_1(0)}\hat{e}_2^n(A) + \frac{\frac{1-\varrho_2}{2\pi}\hat{P}_1(\omega) * \hat{e}_1^n(A) + \frac{1-\varrho_2^l}{2\pi} j\mathcal{P}_1^l(\omega) * (\omega\hat{e}_1^n(A))}{\hat{S}_2(\omega) + \hat{S}_1(0)}. \tag{70}$$

The (implicit) solution to the interface function in the inner/outer BVPs with RR-SP2 are:

$$\begin{aligned}\hat{e}_1^{n+1}(A) =& \frac{-\hat{S}_2(\omega) + \hat{S}_2(0) + \frac{1}{2}\omega^2\hat{S}_{2\omega\omega}(0)}{\hat{S}_1(\omega) + \hat{S}_2(0) + \frac{1}{2}\omega^2\hat{S}_{2\omega\omega}(0)}\hat{e}_2^n(A) + \\ & \frac{\frac{1-\varrho_1}{2\pi}\hat{P}_2(\omega) * \hat{e}_2^n(A) + \frac{1-\varrho_1^l}{2\pi} j\mathcal{P}_2^l(\omega) * (\omega\hat{e}_2^n(A)) - \frac{1-\varrho_1^q}{4\pi}\mathcal{P}_2^q(\omega) * (\omega^2\hat{e}_2^n(A))}{\hat{S}_1(\omega) + \hat{S}_2(0) + \frac{1}{2}\omega^2\hat{S}_{2\omega\omega}(0)},\end{aligned} \tag{71}$$

$$\begin{aligned}\hat{e}_2^{n+1}(A) =& \frac{-\hat{S}_1(\omega) + \hat{S}_1(0) + \frac{1}{2}\omega^2\hat{S}_{1\omega\omega}(0)}{\hat{S}_2(\omega) + \hat{S}_1(0) + \frac{1}{2}\omega^2\hat{S}_{1\omega\omega}(0)}\hat{e}_2^n(A) + \\ & \frac{\frac{1-\varrho_2}{2\pi}\hat{P}_1(\omega) * \hat{e}_1^n(A) + \frac{1-\varrho_2^l}{2\pi} j\mathcal{P}_1^l(\omega) * (\omega\hat{e}_1^n(A)) - \frac{1-\varrho_2^q}{4\pi}\mathcal{P}_1^q(\omega) * (\omega^2\hat{e}_1^n(A))}{\hat{S}_2(\omega) + \hat{S}_1(0) + \frac{1}{2}\omega^2\hat{S}_{1\omega\omega}(0)}.\end{aligned} \tag{72}$$

The first term on the r.h.s. of the above equations is the convergence rate obtained by standard approach, and the second term represents the contribution of the boundary effect. The key terms to evaluate the boundary effect of RR-SP1 and RR-SP2 are:

$$(1 - \varrho_j)\frac{\hat{P}_i * \hat{e}_i^n(A)}{\hat{e}_i^n(A)} + (1 - \varrho_j^l)\frac{j\hat{\mathcal{P}}_i^l * (\omega\hat{e}_i^n(A))}{\hat{e}_i^n(A)}, \quad \text{(RR-SP1)} \tag{73}$$

$$(1 - \varrho_j)\frac{\hat{P}_i * \hat{e}_i^n(A)}{\hat{e}_i^n(A)} + (1 - \varrho_j^l)\frac{j\hat{\mathcal{P}}_i^l * (\omega\hat{e}_i^n(A))}{\hat{e}_i^n(A)} + (1 - \varrho_j^q)\frac{-\frac{1}{2}\hat{\mathcal{P}}_i^q * (\omega^2\hat{e}_i^n(A))}{\hat{e}_i^n(A)}. \quad \text{(RR-SP2)} \tag{74}$$

The calculation of the formula is case-dependent because the error function $\hat{e}_i^n$ is incorporated in the expressions.

4.3. Model study of the boundary effect

In this subsection, we estimate the boundary effect of RR-SP0 as shown in Eq.(58) through a model study. It is noted again that similar strategy is adopted in Subsection 3.2, but serves different

purpose. The estimated calculation follows the modelling of two functions: the spike function $\hat{P}_i$ and the error function $\hat{e}_i^n$ on the interface.

We assume that the error function could be modelled by polynomials up to order three:

$$e(x) \approx a_0 + a_1 x + a_2 x^2 + a_3 x^3,\ x \in (0, L). \tag{75}$$

The Fourier transform of each basis functions is:

$$\mathcal{F}[1] = \frac{\sin\omega}{\omega} + j\frac{cos\omega - 1}{\omega}, \tag{76}$$

$$\mathcal{F}[x] = \frac{sin\omega}{\omega} + \frac{\cos\omega - 1}{\omega^2} + j(\frac{\cos\omega}{\omega} - \frac{\sin\omega}{\omega^2}), \tag{77}$$

$$\mathcal{F}[x^2] = \frac{\sin\omega}{\omega} + \frac{2\cos\omega}{\omega^2} - \frac{2\sin\omega}{\omega^3} + j(\frac{\cos\omega}{\omega} - \frac{2\sin\omega}{\omega^2} - \frac{2(\cos\omega - 1)}{\omega^3}), \tag{78}$$

$$\mathcal{F}[x^3] = \tfrac{\sin\omega}{\omega} + \tfrac{3\cos\omega}{\omega^2} - \tfrac{6\sin\omega}{\omega^3} - \tfrac{6(\cos\omega-1)}{\omega^4} + j(\tfrac{\cos\omega}{\omega} - \tfrac{3\sin\omega}{\omega^2} - \tfrac{6\cos\omega}{\omega^3} + \tfrac{6\sin\omega}{\omega^4}). \tag{79}$$

The energy spectra of the basic functions I, x, x^2 and x^3 are illustrated in Fig.1, where L is assumed equal to 1. This figure shows that most of the energy is distributed in the low wave number zone. In addition, the larger L gets, the narrower the "low wave number band" and the higher the peak value become. The standard of "low" or "high" may vary with analysis error tolerance. In this paper, wave numbers larger than $6\pi/L$ are dropped.

The Fourier transform of different basis functions could be modelled in uniform manner:

$$g_r := \mathcal{F}[e_i^n(A)]_r \approx \frac{L_r}{\omega^{N_r} + 1} cos(\omega + \omega_0^r) \quad \text{all orders}, \tag{80}$$

$$g_i := \begin{cases} \mathcal{F}[e_i^n(A)]_i \approx \frac{L_i}{\omega^{N_i}+1}(\cos(\xi\omega + \omega_0^i) - 1) & \text{order} = 0, \\ \mathcal{F}[e_i^n(A)]_i \approx \frac{L_i}{\omega^{N_i}+1}\cos(\xi\omega + \omega_0^i) & \text{order} \neq 0. \end{cases} \tag{81}$$

The free parameters are $L_r, L_i, N_r, N_i, \xi, \omega_0^r$ and ω_0^i.

Next, we consider the boundary effect. This effect (i.e., the spike function) mostly occurs at the vicinity of the boundaries (see Fig.8) and can be modelled by the exponential functions:

$$P_i(x) \approx \alpha(e^{-\beta(x-\sigma_l)} + e^{\beta(x-\sigma_r)}),\ x \in [\sigma_l,\ \sigma_r]. \tag{82}$$

The Fourier transform of P_i is:

$$\begin{aligned} \mathcal{F}[P_i] := \hat{P}_i =& \frac{\alpha}{\beta^2 + \omega^2}[\beta(\cos\sigma_l\omega + \cos\sigma_r\omega) + \omega(\sin\sigma_r\omega - \sin\sigma_l\omega)] + \\ & \frac{j\alpha}{\beta^2 + \omega^2}[-\beta(\sin\sigma_l\omega + \sin\sigma_r\omega) + \omega(\cos\sigma_r\omega - \cos\sigma_l\omega)], \\ \approx & \frac{\alpha}{\beta}\frac{l_r}{1 + \omega^{n_r}}\cos(\omega + \omega_{0p}^r) + \frac{\alpha}{\beta}\frac{l_i}{1 + \omega^{n_i}}(\cos(\omega + \omega_{0p}^i) - 1)j. \\ :=& f_r + f_i j. \end{aligned} \tag{83}$$

The free parameters are $l_r, l_i, n_r, n_i, \omega_{0p}^r$ and ω_{0p}^i.

With the modelled error function and the spike function, the estimated calculation of Eq.(58) could be performed as follows (see Appendix B for details):

$$(1 - \varrho_j)\frac{\hat{P}_i * \hat{e}_i^n(A)}{\hat{e}_i^n(A)} = \frac{\alpha l(1 - \varrho_j)}{\beta}((\Phi_1 + \Phi_2) + (\Phi_3 + \Phi_4)j), \tag{84}$$

where

$$l = (l_r + l_i)/2,$$

$$\Phi_1 = \frac{\cos(\omega_0^r + \omega)(V_1 + \frac{\omega\cos(\omega_{0p}^r + \omega_0^r + \omega)}{2})}{\cos^2(\omega_0^r + \omega) + \cos^2(\omega_i + \omega)},\ \Phi_2 = \frac{-\cos(\omega_0^i + \omega)(V_2 + \frac{\omega\cos(\omega_{0p}^i + \omega_0^r + \omega)}{2})}{\cos^2(\omega_0^r + \omega) + \cos^2(\omega_0^i + \omega)},$$

$$\Phi_3 = \frac{-\cos(\omega_0^i + \omega)(V_3 + \frac{\omega\cos(\omega_{0p}^r + \omega_0^r + \omega)}{2})}{\cos^2(\omega_0^r + \omega) + \cos^2(\omega_0^i + \omega)},\ \Phi_4 = \frac{\cos(\omega_0^r + \omega)(V_4 + \frac{\omega\cos(\omega_{0p}^i + \omega_0^r + \omega)}{2})}{\cos^2(\omega_0^r + \omega) + \cos^2(\omega_0^i + \omega)}.$$

We recall in Eq.(56) and Eq.(57) that the following term is supposed to compare with the numerator of ρ_i^* : $-\hat{S}_i(\omega) + \hat{S}_i(0)$, which is approximated equal to $-\omega$:

$$\frac{\alpha l(1-\varrho_j)}{2\beta\pi}((\Phi_1+\Phi_2)+(\Phi_3+\Phi_4)j). \tag{85}$$

It is noted that $V_i(\omega)$ $(i = 1, 2, 3, 4)$ is a composite trigonometric function whose magnitude is no greater than three, and we estimate it as $3\sin(\omega)$ (for the expression of this function and its derivation, see Appendix B). The profiles of $1.5(\Phi_1+\Phi_2)$ and $1.5(\Phi_3+\Phi_4)$ are both plotted in Fig.9. Here we assume that $|(\alpha l(1-\varrho_j))/(2\beta\pi)| = 1.5$, although we do not really know it so far. This figure shows that on global scale both $\Phi_1 + \Phi_2$ and $\Phi_3 + \Phi_4$ grows linearly with ω despite constant local oscillation. Therefore, the boundary effect intensity depends on $(\alpha l(1-\varrho_j))/(2\beta\pi)$. Furthermore, since the magnitude of ϱ_j is constrained: $|\varrho_j| < 1$ as earlier mentioned, see Eq.(55), the boundary effect intensity mainly depends on $\alpha l/(2\beta\pi)$. In other words, the boundary effect intensity could be evaluated once the spike function is known.

The reason of assuming that $|(\alpha l(1-\varrho_j))/(2\beta\pi)| = 1.5$ is that this case demonstrates a good example of Eq.(85) counteracting the numerator of ρ_i^* : $-\hat{S}_i(\omega) + \hat{S}_i(0)$. The term $-\hat{S}_i(\omega) + \hat{S}_i(0)$ is considered as a linear function in Fig.9: $y = \pm\omega$ (for magnitude comparison reason we plot both positive and negative cases). In the figure, at $\omega = \pi, 2\pi, ...$, $\Phi_1 + \Phi_2$ is close to zero and $\Phi_3 + \Phi_4$ is nearly equal to ω. It is possible that $\Phi_3 + \Phi_4$ dominates the real part of Eq.(85) and $\Phi_1 + \Phi_2$ dominates the imaginary part. In this case, $\Phi_3 + \Phi_4$ significantly offsets $-\hat{S}_i(\omega) + \hat{S}_i(0)$ and $\Phi_1 + \Phi_2$ is negligible in magnitude, so the standard convergence rate is reduced due to the boundary effect. On the contrary, if $\Phi_1 + \Phi_2$ dominates the real part and $\Phi_3 + \Phi_4$ dominates the imaginary part, the standard convergence rate would be significantly increased due to the boundary effect.

To sum up, if the boundary effect improves the standard convergence rate, it is preferred that $|(\alpha l(1-\varrho_j))/(2\beta\pi)|$ is close to 1.5. This could be used as an empirical rule in the evaluation of the boundary effect for the Poisson's equation.

It is noted that the model study relies on the adopted models and the result is empirical. One may use different models to develop similar evaluation rule. Regardless of the model selections, it is important to provide a practical rule for evaluating the boundary effect.

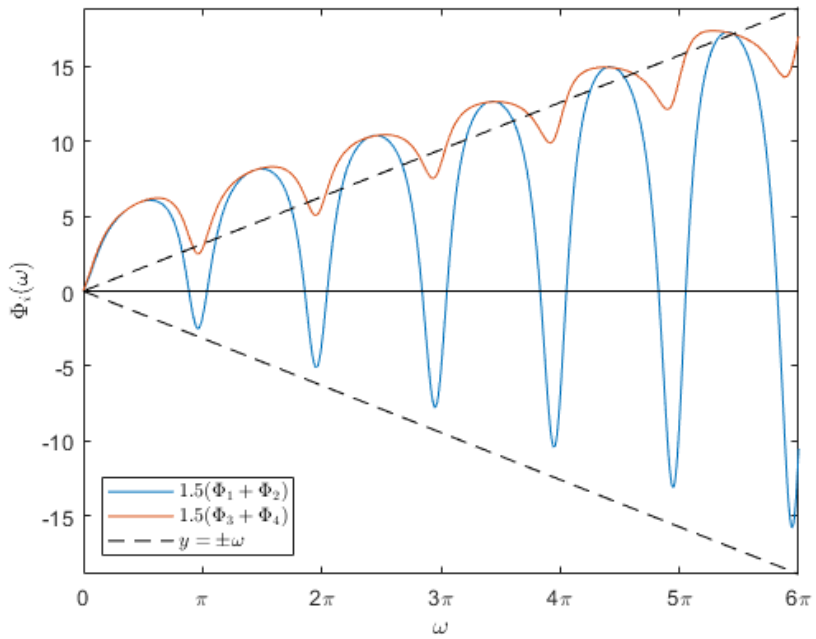


Figure 9: Profiles of $1.5(\Phi_1 + \Phi_2)$ and $1.5(\Phi_3 + \Phi_4)$ as opposed to $\pm\omega$.

5. Numerical tests

In this section, we perform several numerical tests to verify the analytical convergence analysis in application to both a Poisson's equation and a model equation of wall-bounded turbulent flow.

5.1. Poisson's equation

In this subsection, we consider the Poisson's equation, see Eq.(3). The equation is defined in the square domain $[1 \times 1]$ and the boundary conditions are exact. It is given that $f = 20(y^2(1-y) + (3y-1)x(1-x))$, and the exact solution is $u = 10x(1-x)y^2(1-y)$. The mesh is uniform with 65 nodes in each direction. The interface boundary is evenly distributed at $y = A = 1/8, 2/8...7/8$ respectively. The convergence criterion is:

$$\max\left(\left\|\frac{e_1^{n+1}-e_1^n}{e_1^{n+1}}\right\|_\infty, \left\|\frac{e_2^{n+1}-e_2^n}{e_2^{n+1}}\right\|_\infty\right) < 10^{-3} \quad \text{on } \Gamma. \tag{86}$$

Note that the Poisson equation was considered in [22], including the mesh scheme and the convergence criterion.

The Poisson's equation is solved by RR-SP0, RR-SP1 and RR-SP2 respectively. In the test, I, x and x^2 are assumed to be defined in $\mathbb{R}$, which follows the standard convergence rate calculation. In practice, it is implemented by calculating $S_i[I]$ ($S_i[x], S_i[x^2]$) in a wide domain range $x \in [-5, 5]$ so that the boundary effect is too far to affect the concerned domain $[0, 1]$. The algorithms with the standard approach treatment are denoted by RR-SPN*. The numerical test results are shown in Tab. 1. The numerical test result verifies the following theoretical analysis:

1. The convergence rate of RR-SP1* is completely equivalent to that of RR-SP0*.
2. The convergence rate of RR-SP2* is lower than that of RR-SP0* and RR-SP1*.
3. The convergence rate of RR-SP0* and RR-SP1* could be accurately evaluated by $\Delta s_1(\omega)\Delta s_2(\omega)$.
4. The convergence rate of RR-SP2* could be accurately evaluated by $\prod_1^2 \Delta s_{i\omega\omega}(\omega)$ (or $\prod_1^2 \Delta s_{i\omega\omega}(0)$).
5. The convergence rate of the algorithms is symmetric about $A = 4/8$.

Table 1: Convergence iterations of RR-SPN* in application to the Poisson's equation.

A	1/8	2/8	3/8	4/8	5/8	6/8	7/8
RR-SP0*	12	16	17	18	17	15	11
RR-SP1*	12	16	17	18	17	15	11
RR-SP2*	11	13	15	15	15	13	11

Here are the elaborations:

The numbers of iterations of RR-SP1* are exactly equal to those of RR-SP0*, indicating that they have the same convergence rate, as was previously analysed. Regardless of A, RR-SP2* has smaller (or equal) numbers of iterations as opposed to RR-SP0* and RR-SP1*, indicating the lower convergence rate of RR-SP2*. The iteration numbers of the three algorithms increase with rising A from 1/8 to 4/8, which is reflected from Figs.3. In addition, for all the three algorithms, the iteration number of $A = 7/8$ is nearly equal to $A = 1/8$, and so are $A = (2/8, 6/8)$, $A = (3/8, 5/8)$ cases. It could be interpreted as a reflection of the 'symmetric' property of $\hat{S}_1$ and $\hat{S}_2$ in terms of A. From the definition of $\hat{S}_i$, it is seen that $\hat{S}_{1|A=A^*}(\omega_0) = \hat{S}_{2|A=1-A^*}(\omega_0)$. As a result $\Delta s_{1|A=A^*}\Delta s_{2|A=A^*} = \Delta s_{2|A=1-A^*}\Delta s_{1|A=1-A^*}$, and so is true for $\prod_1^2 \Delta s_{i\omega\omega}(\omega)$.

Next, we solve the Poisson's equation with RR-SP0, RR-SP1 and RR-SP2. The results of this test are shown in Tab. 2. Compared with the result in Tab. 1, the following conclusions are drawn:

1. Boundary effect improves the convergence for all the three algorithms.
2. The boundary effect intensity of RR-SP0 could be evaluated by modelling the spike function

according to Eq.(82) and Eq.(83).

Table 2: Convergence iterations of RR-SPN in application to the Poisson's equation.

A	1/8	2/8	3/8	4/8	5/8	6/8	7/8
RR-SP0	8	9	9	9	8	8	7
RR-SP1	6	7	7	7	7	7	6
RR-SP2	6	7	7	7	6	6	6

Table 3: CPU time ($\times 10^{-2}$s) of RR-SPN* and RR-SPN in application to the Poisson's equation.

A	1/8	2/8	3/8	4/8	5/8	6/8	7/8
RR-SP0*	10(10)	16(18)	18(22)	19(24)	18(22)	16(18)	9.9(10)
RR-SP1*	10(10)	16(18)	18(22)	19(24)	18(23)	17(18)	10(10)
RR-SP2*	6.1(5)	5.3(5)	5.6(6)	5.4(6)	5.5(6)	5.3(5)	5.5(5)
RR-SP0	7.3(7)	7.6(8)	6.7(7)	6.2(7)	6.3(7)	6.1(6)	6.4(6)
RR-SP1	5.4(5)	6.2(6)	5.6(6)	5.3(6)	5.8(6)	5.2(5)	5.5(5)
RR-SP2	4.8(4)	4.6(4)	4.1(4)	4.0(4)	4.0(4)	3.4(3)	3.7(3)

Here are the elaborations:

The iteration numbers of all the three algorithms reduce significantly after boundary effect is incorporated. This shows that the boundary effect positively affects the convergence. Further, it reveals the limitation of the standard approach and highlights the significance of considering the boundary effect.

In the test of RR-SP0, the iteration numbers reduce by 4,7,8,9 iterations, respectively, for $A = 1/8, 2/8, 3/8$ and $4/8$ cases. Clearly, the boundary effect strength is influenced by A. The profiles of the spike functions for $A = 1/8, 3/8$ and $7/8$ cases are plotted in Figs 10 &11. It is seen that $A = 3/8$ case has one "taller and wider" spike function in both $S_1 I$ and $S_2 I$ profiles, with $|(\alpha l(1 - \varrho_j))/(2\beta\pi)| \approx 1.8$ if assuming $|1 - \varrho_j| = 2$. For $A = 1/8$ case, it has one "shorter and thinner" spike function ($|(\alpha l(1 - \varrho_j))/(2\beta\pi)| \approx 0.2$) for $S_1 I$ profile and one "taller and wider" spike function for $S_2 I$. The case of $A = 7/8$ is similar to $A = 1/8$. Since the "taller and wider" spike function has the closer value of $|(\alpha l(1 - \varrho_j))/(2\beta\pi)|$ to 1.5, as the theoretical estimation suggests in Subsection 4.3, the standard convergence of $A = 3/8$ case is better improved by the boundary effect.

The computational cost for evaluating the boundary effect of RR-SP0 is low: merely by computing the SP operators applied to the unit function and modelling the spike function. The computation of the SP operators is required for the implementation of the algorithm, so only the modelling cost is incurred.

In Tab.3, the computational time (CPU time) is displayed for all the algorithms with various A. The number in the parenthesis represents the iteration number. It is noted that the data in Tab.3 are obtained using the newly written code with PETSC library. The data of Tabs. 2 and 1 are obtained from the previously written code that did not employ PETSC. The two codes show similar result despite the criteria to check the convergence is sightly different. Tab.3 shows that the CPU time is nearly proportional to the iteration numbers. In other words, each iteration takes roughly the same amount of computational efforts (time) as a result of each single algorithm producing the linear system of similar complexity. Therefore, the iteration number could be used as a reliable indicator to measure the algorithm efficiency.

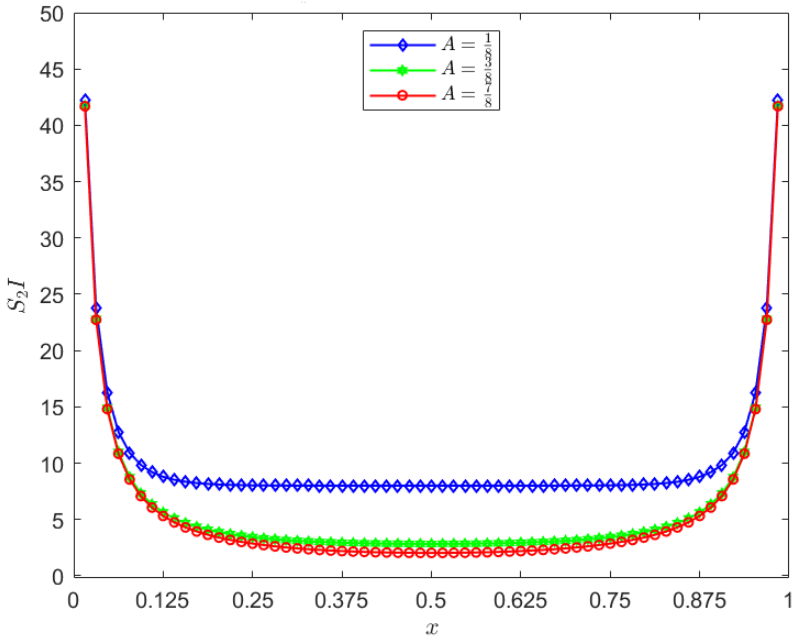


Figure 10: Profiles of $S_1[I]$ (strictly I') in application to the Poisson's equation with $A = 1/8, 3/8$ and $7/8$.

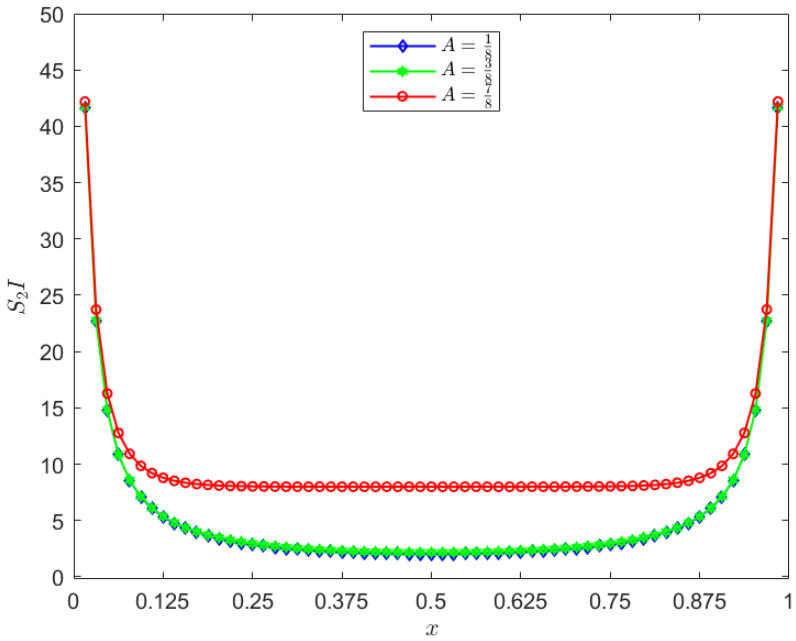


Figure 11: Profiles of $S_2[I]$ (strictly I') in application to the Poisson's equation with $A = 1/8, 3/8$ and $7/8$.

5.2. Model equation

Finally, we consider the model equation that was also considered in [7, 22]. This equation is a linear model of the momentum balance of fluid adopted by the Reynolds-Averaged-Navier-Stokes (RANS) approach in turbulent modelling. First let us recall the model equation:

$$\begin{aligned}(\mu U_y)_y + \sigma U_{xx} + \beta U_y + \gamma U = f(x,y),\\ U(x,0) = 0, \quad U(x,1) = U_s(x),\\ U(0,y) = U_0(y), \quad U(1,y) = U_1(y),\end{aligned} \tag{87}$$

where $\sigma = \alpha\mu$, $\mu = \frac{1-e^{y/\epsilon}+\delta}{Re}$, $\epsilon = 3\times 10^{-2}$, $\delta = 10^{-2}$, $\beta = y$, $\gamma = -y^2$, $Re = 10^4$, $f = -100x^2$, $U_s = 1 + 100x^2$. The definitions of U_0 and U_1 are given in Eq.(43) of [7]. The convergence criterion is:

$$\max\left(\frac{\|e_1^{n+1} - e_1^n\|_\infty}{\|e_1^{n+1}\|_\infty}, \frac{\|e_2^{n+1} - e_2^n\|_\infty}{\|e_2^{n+1}\|_\infty}\right) < 10^{-6} \quad \text{on } \Gamma. \tag{88}$$

The model equation is solved by both RR-SPN* and RR-SPN algorithms. The numerical test result is shown in Tab. 4. The following conclusions are drawn:

1. The standard convergence analysis result drawn from the Poisson's equation also applies to the model equation, although the latter does not have a variable-separated form.
2. The boundary effect could negatively affect the convergence occasionally, for example, RR-SP1.
3. The boundary effect is essentially part of the nonlocal effect of the problem.
4. The overall nonlocal effect of the problem results from both the governing equation and the boundary effect.

Table 4: Convergence iteration of (sequential) RR-SPN (N=0,1,2) and RR-SPN* in comparison to solve a model equation, $A = 10^{-3}$.

α	1	10^2	10^4
RR-SP0	3	7	10
RR-SP0*	4	8	16
RR-SP1	3	8	44
RR-SP1*	4	8	16
RR-SP2	3	4	10
RR-SP2*	4	5	15

Here are the elaborations:

Although the analytical calculation of the convergence rate for the model equation is not feasible, the numerical result of the model equation still complies with the analysis result of the Poisson's equation: the iteration numbers of RR-SP1* are entirely equal to those of RR-SP0*, and they are slightly larger than (or equal to) those of RR-SP2*. It suggests a substantial similarity between the SP operators' eigenvalues (symbols) of the two cases: the Poisson's equation and the model equation. Although the eigenvalues (symbols) in application to the model equation are challenging to obtain analytically, they could be treated analogously to the Poisson's equation. To demonstrate this, we consider the inverse Fourier transform upon the assumption that I is defined in $\mathbb{R}$:

$$\mathcal{F}[S_i[I]] = 2\pi\hat{S}_i(\omega,x)\delta(\omega) \xrightarrow[\text{Fourier}]{\text{Inverse}} S_i[I] = \hat{S}_i(0,x). \tag{89}$$

In the general case, the eigenvalue (symbol) should be related to both ω and x, as is shown in the general form, see Eq.(A.1). However, for the Poisson's equation, the eigenvalue is merely a function of ω and independent from x (see Eq.(14)) due to the separation of variables. The same x-independency is also observed for the eigenvalue (symbol) in the model equation case, see Figs.12-14. According to the plots on these figures, the $S_i[I]$ profiles remain constant (independent from x)

in the far off-boundary zone. This suggests that the model equation has variable-separation form solution as well. Therefore, the eigenvalues (symbols) of the model equation could be treated in an analogous way to the Poisson's equation. In other words, all the convergence analysis results obtained by the standard approach for the Poisson's equation could also be applied to the model equation since the convergence rate of the algorithms depends on $\hat{S}_i(\omega)$ and its derivatives only. This extends the applicability of the theoretical result drawn from the well-understood Poisson's equation to the less-understood model equation. Additionally, this result could be further extended to other complex equations at the mere cost of computing $S_i[I]$.

Next, we consider the cases with various α. The three values simulate three scenarios where the nonlocal effect of the problem is weak, medium and strong.

In the case of $\alpha = 1$, there is hardly any nonlocal effect, and the problem is essentially one-dimensional, so $S_i[I] \approx S_i^*[I]$, $S_i[x] \approx xS_i^*[I]$ and $S_i[x^2] \approx x^2 S_i^*[I]$. As a result, $T_{il} = T_{iq} \equiv 0$. The algorithms of RR-SP1 and RR-SP2 are simply reduced to RR-SP0. This is the reason that all the three algorithms yield equivalent iterations with the standard approach. Meanwhile, the difference between RR-SPN and RR-SPN* is minor since the boundary effect is feeble (see Fig.12).

In the case of $\alpha = 10^2$, the intensity of the nonlocal effect grows,and the problem is no longer one-dimensional. On the one hand, the boundary effect remains limited (see Fig.13), so no remarkable difference between RR-SPN and RR-SPN* cases is seen. On the other hand, as the theoretical analysis of the standard approach suggests, the convergence rate of RR-SP2* is lower than the other two. That is why RR-SP2* converges with significantly fewer iterations (3) than its counterparts.

In the case of $\alpha = 10^4$, the nonlocal effect keeps growing, and the boundary effect becomes strong (see Fig.14). The boundary effect is reflected by the significant difference between RR-SPN and RR-SPN* cases. Meanwhile, for standard approach cases, RR-SP2* shows fewer iteration numbers due to the same reason as provided by the theoretical analysis of the standard approach.

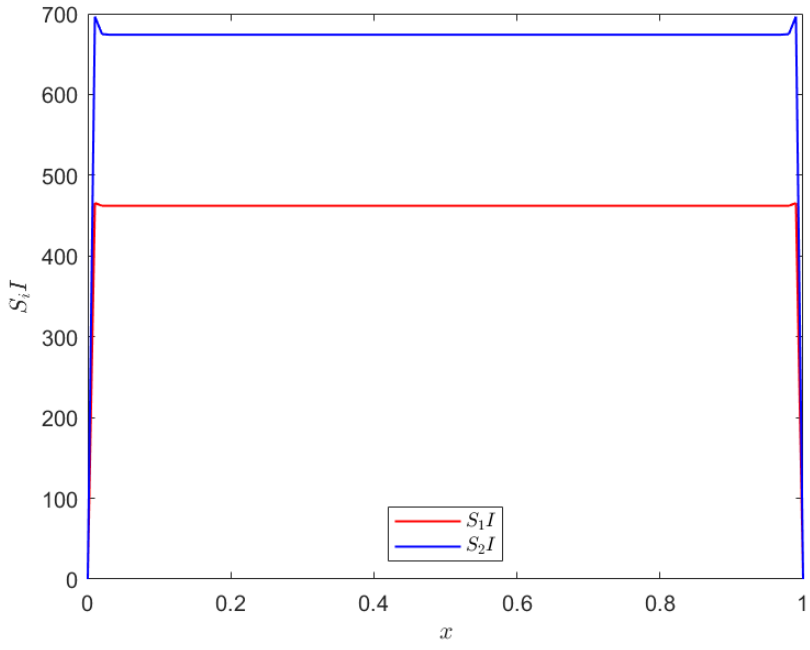


Figure 12: Profiles of $S_i[I]$ $(i = 1, 2)$ in application to the model equation, $\alpha = 1$.

The results of the numerical tests show that the boundary effect improves the standard convergence rate. The reason is that the boundary effect is one part of the nonlocal effect of the problem. Fig.12 shows that in the case of $\alpha = 1$, the spike function (boundary effect) hardly exists. It suggests that the boundary effect intensity is consistent with the intensity of the nonlocal effect. The approximation of the SP operator is realized by expanding the interface function into the Taylor

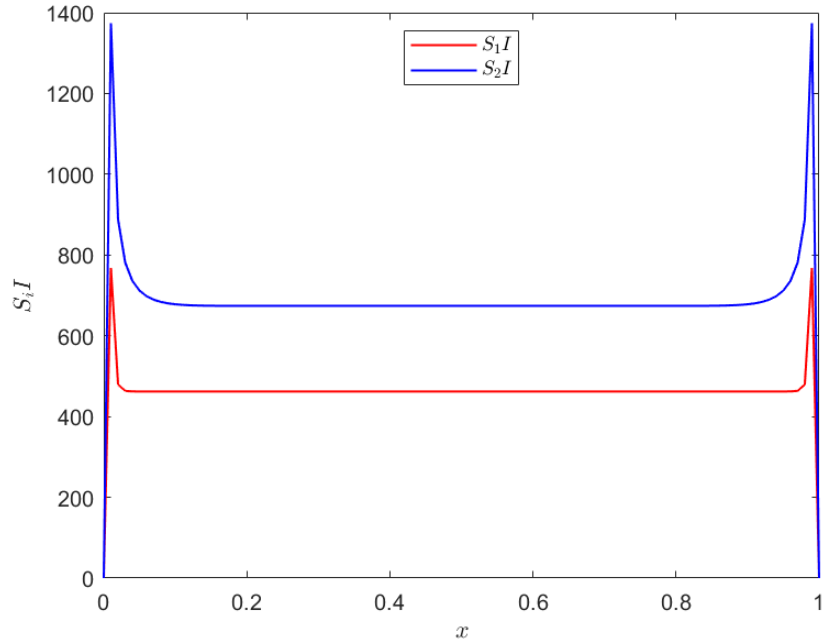


Figure 13: Profiles of $S_i[I]$ $(i = 1, 2)$ in application to the model equation, $\alpha = 10^2$.

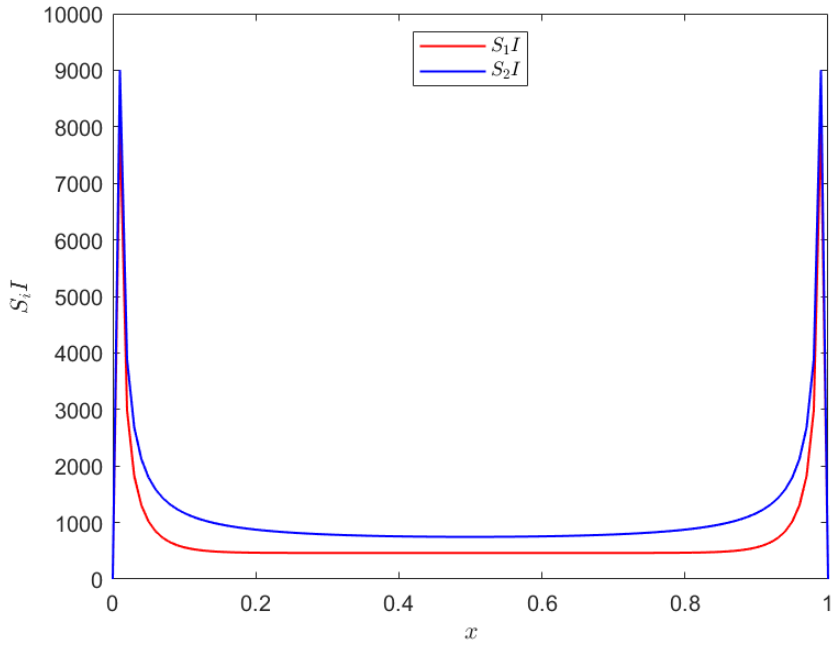


Figure 14: Profiles of $S_i[I]$ $(i = 1, 2)$ in application to the model equation, $\alpha = 10^4$.

series: $S_i[f] \to S_i[\{I, x, x^2\}_T]$, where $\{...\}_T$ represents the Taylor expansion terms. The boundary effect in $S_i[I], S_i[x]$ and $S_i[x^2]$ are components of the boundary effect in $S_i[f]$, which is essentially part of the nonlocal effect of the given problem. We deduce that if the original problem is defined in $\mathbb{R}$, there would be no need to consider the boundary effect at any level: I, x and x^2 are all in $\mathbb{R}$ and the convergence calculation by the standard approach is equivalent to the actual calculation.

The other part of the nonlocal effect of the problem results from the governing equation, which corresponds to the standard approach. As mentioned above, for the case of $\alpha = 1$ of the model equation, this is a (quasi) one-dimensional problem. As a result, $S_i[I] = S_i^*[I]$, $S_i[x] = xS_i^*[I]$ and $S_i[x^2] = x^2 S_i^*[I]$. For larger α, the algorithm of RR-SP2* is proven to have a lower convergence rate than its counterparts because it captures more of the nonlocal nature of the governing equation by increasing the number of the terms in the Taylor series that we keep. (However, keeping more terms may not always be effective in capturing better the nonlocal effect, such as RR-SP1* making no difference from RR-SP0*.)

We conclude that the nonlocal effect of the problem is reflected in two parts: the governing equation and the boundary effect. Then, Tab. 4 could be interpreted as follows: in the case of weak nonlocal effect, the three algorithms are essentially equivalent because no nonlocal effect needs to be captured on the interface. In the case of moderate nonlocal effect, RR-SP2* performs better in capturing the nonlocal effect on the governing equation level, so it converges faster than the other two counterparts. The boundary effect does not have a remarkable influence in this case. In the case of strong nonlocal effect, the boundary effect significantly influences the convergence, and it is demonstrated to be positive.

It is noted that the unconventionally slow convergence of RR-SP1 in $\alpha = 10^4$ case is due to the boundary effect of the algorithm, because the slow convergence is not observed for RR-SP1* in the same case. However, it remains challenging to calculate precisely the strength of the boundary effect, which is given by Eq. (73). In Section 4.3, we estimate the strength of the boundary effect of RR-SP0 through model work, but the approach is expected to become much more complex and likely to incur larger errors for RR-SP1. We plan to address the problem in the future work.

Meanwhile, to independently check this unusual piece of data, we write new code using PETSC library to replicate the test of $\alpha = 10^4$. The new code shows highly similar result: iteration numbers are 10, 31 and 9 for RR-SP0, RR-SP1 and RR-SP2 respectively. The difference of the result between the two versions of the code could be possibly due to different KSP (Krylov subspace) solver parameters setup and preconditioning techniques adapted by the two codes: the old code used in-house KSP solver/preconditioner while the new code benefits from the well-developed PETSC library. The algorithm with slow convergence (RR-SP1) seems more sensitive to the minor change of other factors. If we relax the convergence criterion from Eq.(86) to Eq.(88) and maintain everything else the same, the iteration numbers become 5, 9, 5 for RR-SP0, RR-SP1 and RR-SP2 respectively. Again, RR-SP1 is the slowest in converging, but the iteration number differs not as much as in Tab.4.

6. Conclusions

In this paper, we have presented a comprehensive convergence analysis of a domain decomposition method with nonlocal interface boundary conditions based on [22]. The convergence rate calculation is performed on the Poisson's equation with Fourier transform, assuming the boundaries being put at infinity (standard approach). Then, the analysis considers the boundary effect through a model study. The standard approach reveals the nonlocal effect of the problem reflected in the governing equation. The boundary effect analysis considers the nonlocal effect reflected in the boundary conditions. Together, they compose the entire convergence analysis of the domain decomposition method.

On the governing equation level, the symbols of the SP operators completely determine the convergence rate of the domain decomposition method. The method's convergence could be effectively

evaluated by algebraic treatment of the symbols (and derivatives). At the boundary condition level, the boundary effect is supposed to improve the convergence, and the intensity could be evaluated at a low computational cost.

Practically, the analysis result based on the Poisson's equation is applied to resolving the modelled momentum equation of viscous fluid flow, and can be further applied to other complex problems in the future, for instance, [4, 5]. The theoretical study of the Poisson's equation provides a blueprint for similar analyses of more complexity. Therefore, the applicability of the domain decomposition method is significantly extended.

Acknowledgements

The first author acknowledges the constructive remarks made by Dr. S. Utyuzhnikov from the University of Manchester. The authors gratefully acknowledge the financial support provided by the Belgian Federal Public Service Economy under the Energy Transition Fund, project SFP-LOCA.

References

[1] B. Aksoylu, M. Parks, Towards domain decomposition for nonlocal problems, Tech. rep., Technical Report (2009).

[2] B. Aksoylu, M. L. Parks, Variational theory and domain decomposition for nonlocal problems, Applied Mathematics and Computation 217 (14) (2011) 6498–6515.

[3] X. Xu, C. Glusa, M. D'Elia, J. T. Foster, A FETI approach to domain decomposition for meshfree discretizations of nonlocal problems, Computer Methods in Applied Mechanics and Engineering 387 (2021) 114148.

[4] A. Ellabib, A. Nachaoui, A. Ousaadane, Mathematical analysis and simulation of fixed point formulation of cauchy problem in linear elasticity, Mathematics and Computers in Simulation 187 (2021) 231–247.

[5] A. Ellabib, A. Nachaoui, A. Ousaadane, Convergence study and regularizing property of a modified robin–robin method for the cauchy problem in linear elasticity, Inverse Problems 38 (7) (2022) 075007.

[6] R. C. Kirby, A. Klöckner, B. Sepanski, Finite elements for Helmholtz equations with a nonlocal boundary condition, SIAM Journal on Scientific Computing 43 (3) (2021) A1671–A1691.

[7] S. Utyuzhnikov, Domain decomposition for near-wall turbulent flows, Computers & Fluids 38 (9) (2009) 1710–1717.

[8] F. Nataf, Interface connections in domain decomposition methods, in: Modern Methods in Scientific Computing and Applications, Springer, 2002, pp. 323–364.

[9] A. Yesypenko, P.-G. Martinsson, Parallel optimizations for the hierarchical Poincaré-Steklov scheme (HPS), arXiv preprint arXiv:2211.14969 (2022).

[10] T.-T.-P. Hoang, Fully implicit local time-stepping methods for advection-diffusion problems in mixed formulations, Computers and Mathematics with Applications 118 (C) (2022) 248–264.

[11] A. Quarteroni, A. Valli, Domain decomposition methods for partial differential equations, Oxford University Press, 1999.

[12] Q. Hu, Preconditioning Poincaré–Steklov operators arising from domain decompositions with mortar multipliers, IMA Journal of Numerical Analysis 24 (4) (2004) 643–669.

[13] E. Engström, E. Hansen, Convergence analysis of the nonoverlapping Robin–Robin method for nonlinear elliptic equations, SIAM Journal on Numerical Analysis 60 (2) (2022) 585–605.

[14] E. Engström, E. Hansen, Linearly convergent nonoverlapping domain decomposition methods for quasilinear parabolic equations, arXiv preprint arXiv:2308.15314 (2023).

[15] R. F. Susan-Resiga, H. M. Atassi, A domain decomposition method for the exterior Helmholtz problem, Journal of Computational Physics 147 (2) (1998) 388–401.

[16] R. Natarajan, Domain decomposition using spectral expansions of Steklov–Poincaré operators, SIAM Journal on Scientific Computing 16 (2) (1995) 470–495.

[17] Y. Duan, Y.-j. Tan, Meshless galerkin method based on regions partitioned into subdomains, Applied Mathematics and Computation 162 (1) (2005) 317–327.

[18] B. N. Khoromskij, J. M. Melenk, Boundary concentrated finite element methods, SIAM Journal on Numerical Analysis 41 (1) (2003) 1–36.

[19] D. Koyama, Error estimates of the dtn finite element method for the exterior Helmholtz problem, Journal of Computational and Applied Mathematics 200 (1) (2007) 21–31.

[20] B. N. Khoromskij, G. Wittum, An asymptotically optimal substructuring method for the Stokes equation, in: DD9 Proceedings, Wiley, New York, 1997, p. 31–39.

[21] Y. Zhang, V. Jain, A. Palha, M. Gerritsma, The discrete Steklov–Poincaré operator using algebraic dual polynomials, Computational Methods in Applied Mathematics 19 (3) (2019) 645–661.

[22] S. V. Utyuzhnikov, H. Li, Domain decomposition with nonlocal interface boundary conditions, Journal of Computational and Applied Mathematics. 421 (2023).

[23] J. C. Garay, Asynchronous Optimized Schwarz Methods for Partial Differential Equations in Rectangular Domains, Doctoral dissertation, Temple University, 2018.

[24] B. Lessani, M. V. Papalexandris, Time-accurate calculation of variable density flows with strong temperature gradients and combustion, Journal of Computational Physics 212 (1) (2006) 218–246.

[25] S. H. Lui, On accelerated convergence of nonoverlapping Schwarz methods, Journal of Computational and Applied Mathematics 130 (1-2) (2001) 309–321.

[26] Q. Deng, Timely communicaton: An analysis for a nonoverlapping domain decomposition iterative procedure, SIAM Journal on Scientific Computing 18 (5) (1997) 1517–1525.

[27] W. P. Tang, Generalized schwarz splittings, SIAM Journal on Scientific and Statistical Computing 13 (2) (1992) 573–595.

[28] P. L. Lions, On the Schwarz alternating method III: a variant for nonoverlapping subdomains, in: Third international symposium on domain decomposition methods for partial differential equations, Vol. 6, SIAM Philadelphia, 1990, pp. 202–223.

[29] A. Quarteroni, A. Valli, Theory and application of Steklov-Poincaré operators for boundary-value problems, in: Applied and Industrial Mathematics: Venice-1, 1989, Springer, 1991, pp. 179–203.

[30] M. Ruzhansky, V. Turunen, Pseudo-differential operators and symmetries: background analysis and advanced topics, Vol. 2, Springer Science & Business Media, 2009.

Appendix A. Symbol calculation

The formulae to calculate the symbol $a(x,\omega)$ of a pseudo-differential operator T follows [30]:

$$a(x,\omega) := e^{-2\pi jx\omega} T(e^{2\pi jx\omega}). \tag{A.1}$$

In this case, the pseudo-operator (S_i) operates on y direction at interface $y = A$. First we consider the symbol of S_1. According to the definition of S_1 and its application on the Poisson's equation in Ω_1, the following BVP for calculating $S_1(e^{2\pi jx\omega})$ can be formulated:

$$\begin{aligned} -\nabla^2 e_1^{n+1} &= 0, \quad \text{on } \Omega_1, \\ e_1^{n+1} &= 0, \quad \text{on } \partial\Omega_1/(y = A), \\ e_1^{n+1} &= e^{2\pi jx\omega}, \quad \text{on } y = A. \end{aligned} \tag{A.2}$$

To solve it, we apply Fourier transform w.r.t. x on the BVP defined in Ω_1 to get a reduced one-dimensional BVP:

$$\begin{aligned} \frac{\partial^2 \hat{e}_1^{n+1}}{\partial y^2} - \omega^2 \hat{e}_1^{n+1} &= 0, \\ \hat{e}_1^{n+1}(0) = 0, \quad \hat{e}_1^{n+1}(A) &= 1. \end{aligned} \tag{A.3}$$

The solution to the one-dimensional BVP is

$$\hat{e}_1^{n+1}(\omega, y) = \frac{\sinh(\omega y)}{\sinh(\omega A)}. \tag{A.4}$$

Furthermore, we apply inverse Fourier transform on $\hat{e}_1^{n+1}$ to restore interface solution and take derivative. There is only one harmonic to consider so the integral reduces:

$$e_1^{n+1}(x,y) = \int \hat{e}_1^{n+1}(\omega, y) e^{2\pi jx\omega} d\omega = \hat{e}_1^{n+1}(\omega, y) e^{2\pi jx\omega}. \tag{A.5}$$

$$S_1(e^{2\pi jx\omega}) := e_{1y}^{n+1}(x, A) = e^{2\pi jx\omega} \omega \coth(\omega A). \tag{A.6}$$

Therefore, the symbol $(\hat{S}_1)$ of the operator is

$$\hat{S}_1(\omega) := e^{-2\pi jx\omega} S_1(e^{2\pi jx\omega}) = \omega \coth(\omega A). \tag{A.7}$$

Next, we consider the symbol of S_2. The calculation is almost the same as with $\hat{S}_1$. We apply Fourier transform w.r.t. x on BVP2 defined in Ω_2 to get a reduced one-dimensional BVP:

$$\begin{aligned} \frac{\partial^2 \hat{e}_2^{n+1}}{\partial y^2} - \omega^2 \hat{e}_2^{n+1} &= 0, \\ \hat{e}_2^{n+1}(0) = 0, \quad \hat{e}_2^{n+1}(A - B) &= 1. \end{aligned} \tag{A.8}$$

The solution is

$$\hat{e}_2^{n+1}(\omega, y) = \frac{\sinh(\omega(y - B))}{\sinh(\omega(A - B))}. \tag{A.9}$$

Let us restore the interface solution,

$$e_2^{n+1}(x,y) = \int \hat{e}_2^{n+1}(\omega, y) e^{2\pi jx\omega} d\omega = \hat{e}_2^{n+1}(\omega, y) e^{2\pi jx\omega}. \tag{A.10}$$

$$S_2(e^{2\pi jx\omega}) := -e_{2y}^{n+1}(x, A) = e^{2\pi jx\omega} \omega \coth(\omega(B - A)). \tag{A.11}$$

Therefore, the symbol $(\hat{S}_2)$ of the operator is

$$\hat{S}_2(\omega) := e^{-2\pi jx\omega} S_2(e^{2\pi jx\omega}) = \omega \coth(\omega(B - A)). \tag{A.12}$$

Compare $\hat{S}_i(\omega)$ with the general form of the symbol $a(x,\omega)$, it is seen that $\hat{S}_i$ is not a function of x but only ω. This is still because the solution could be separated in terms of x and y. The separation gives rise to the solution to the reduced one-dimensional BVP w.r.t. y directly, and the solution is free from containing any x.

Appendix B. Convolution calculation

We consider the Fourier transform of the spike function ($\hat{P}_i$) and the error function ($\hat{e}_i^n$). Let us denote $\hat{P}_i(\omega) = f_r(\omega) + f_i(\omega)j$ and $\hat{e}_i^n(A) = g_r(\omega) + g_i(\omega)j$. It is noted that $\hat{e}_i^n(A)$ (hence g_r, g_i) is defined in $[0, 6\pi]$.

$$\begin{aligned}\frac{\hat{P}_i(\omega) * \hat{e}_i^n(A)}{\hat{e}_i^n(A)} =& \frac{g_r(f_r * g_r - f_i * g_i)}{g_r^2 + g_i^2} + \frac{g_i(-f_i * g_r - f_r * g_i)}{g_r^2 + g_i^2} + \\ & (\frac{g_i(f_i * g_i - f_r * g_r)}{g_r^2 + g_i^2} + \frac{g_r(f_i * g_r + f_r * g_i)}{g_r^2 + g_i^2})j.\end{aligned} \tag{B.1}$$

The exact calculation is complicated but since f_r, f_i, g_r and g_i have the same expression (see Eqs.(80),(81),(83)), the calculation is similar in every part and the overall calculation could be simplified. Additionally, since α and β are separated from ω, they could be moved out from convolution calculation. A sample is given below.

$$\begin{aligned}f_r(\omega) * g_r(\omega) &= \int_0^\omega \frac{\alpha}{\beta} \frac{l_r}{1+\tau^{n_r}} \cos(\tau + \omega_{0p}^r) \frac{L_r}{(\omega-\tau)^{N_r}+1} \cos(\xi(\omega-\tau) + \omega_0^r) d\tau \\ &= \frac{\alpha\omega}{\beta}[fg]_{rr}(\omega^*), \qquad (0 \le \omega^* \le \omega)\end{aligned} \tag{B.2}$$

where $[fg]_{rr}(x) := \frac{l_r}{1+x^{n_r}} \cos(x + \omega_{0p}^r) \frac{L_r}{(\omega-x)^{N_r}+1} \cos(\xi(\omega - x) + \omega_0^r)$.

Instead of the mean-value estimation, $f_r(\omega) * g_r(\omega)$ could be estimated in a more precise way:

$$\begin{aligned}f_r(\omega) * g_r(\omega) =& \frac{\alpha}{\beta} \int_0^\omega \frac{l_r}{1+\tau^{n_r}} \cos(\tau + \omega_{0p}^r) \frac{L_r}{(\omega-\tau)^{N_r}+1} \cos(\omega - \tau + \omega_0^r) d\tau \\ <& \frac{\alpha l_r}{\beta} \frac{L_r}{1+\tau^{N_r}} \int_0^\omega \cos(\tau + \omega_{0p}^r) \cos(\omega - \tau + \omega_0^r) d\tau \\ =& \frac{\alpha l_r}{\beta} \frac{L_r}{1+\tau^{N_r}} (\frac{\sin(\omega_{0p}^r - \omega_0^r + \omega)}{4} + \frac{\sin(\omega_0^r - \omega_{0p}^r + \omega)}{4} + \\ & \frac{\omega \cos(\omega_{0p}^r + \omega_0^r + \omega)}{2}) \\ :=& \frac{\alpha}{\beta} \frac{L_r l_r}{1+\tau^{N_r}} [FG]_{rr}(\omega).\end{aligned} \tag{B.3}$$

Similar estimation could be made about $f_i * g_i$:

$$\begin{aligned}f_i(\omega) * g_i(\omega) =& \frac{\alpha}{\beta} \int_0^\omega \frac{l_i}{1+\tau^{n_i}} \cos(\tau + \omega_{0p}^i) \frac{L_i}{(\omega-\tau)^{N_i}+1} (\cos(\xi(\omega-\tau) + \omega_0^i) - 1) d\tau \\ <& \frac{\alpha l_i}{\beta} \frac{L_i}{1+\tau^{N_i}} \int_0^\omega \cos(\tau + \omega_{0p}^i)(\cos(\xi(\omega-\tau) + \omega_0^i) - 1) d\tau \\ =& \frac{\alpha l_i}{\beta} \frac{L_i}{1+\tau^{N_i}} (\frac{\sin(\omega_{0p}^i - \omega_0^i + \xi\omega)}{2(\xi-1)} + \frac{\sin(\omega_{0p}^i - \omega_0^i + \omega)}{2(\xi-1)} - \\ & \sin(\omega_0^i + \xi\omega) + \sin(\omega_0^i) + \frac{\sin(\omega_{0p}^i + \omega_0^i + \xi\omega)}{2(\xi-1)} - \frac{\sin(\omega_{0p}^i + \omega_0^i + \omega)}{2(\xi-1)}) \\ :=& \frac{\alpha}{\beta} \frac{L_i l_i}{1+\tau^{N_i}} [FG]_{ii}(\omega).\end{aligned} \tag{B.4}$$

Therefore, the first term on the right-hand-side of Eq.(B.1) could be estimated:

$$\begin{aligned}& \frac{g_r(f_r * g_r - f_i * g_i)}{g_r^2 + g_i^2} \\ =& \frac{\alpha}{\beta} \frac{g_r(\frac{L_r l_r}{1+\tau^{N_r}} [FG]_{rr}(\omega) - \frac{L_i l_i}{1+\tau^{N_i}} [FG]_{ii}(\omega))}{g_r^2 + g_i^2} \\ \approx& \frac{\alpha l}{\beta} \frac{\cos(\omega + \omega_0^r)([FG]_{rr}(\omega) - [FG]_{ii}(\omega))}{\cos(\omega + \omega_0^r)^2 + \cos(\xi\omega + \omega_0^i)^2} \\ =& \frac{\alpha l}{\beta} \Phi_1(\omega), \quad l = (l_r + l_i)/2\end{aligned} \tag{B.5}$$

where

$$\begin{aligned}\Phi_1(\omega) =&[\cos(\omega_0^r+\omega)(\frac{\sin(\omega_{0p}^r-\omega_0^r+\omega)}{4}+\frac{\sin(\omega_0^r-\omega_{0p}^r+\omega)}{4}-\frac{\sin(\omega_{0p}^i-\omega_0^i+\omega)}{2(\xi+1)}-\\&\frac{\sin(\omega_0^i-\omega_{0p}^i+\xi\omega)}{2(\xi+1)}+\frac{\sin(\omega_0^i+\xi\omega)-\sin(\omega_0^i)}{\xi}+\frac{\omega\cos(\omega_{0p}^r+\omega_0^r+\omega)}{2}-\\&\frac{\sin(\omega_{0p}^i+\omega_0^i+\xi\omega)}{2(\xi-1)}+\frac{\sin(\omega_{0p}^i+\omega_0^i+\omega)}{2(\xi-1)})]/(\cos(\omega_0^r+\omega)^2+\cos(\omega_0^i+\xi\omega)^2).\end{aligned} \tag{B.6}$$

When ω is not too small (for instance, $\omega > \pi$) and $\xi \approx 1$, $\Phi_1(\omega)$ could be estimated as follows:

$$\Phi_1(\omega) \approx \frac{\cos(\omega_0^r+\omega)(V_1+\frac{\omega\cos(\omega_{0p}^r+\omega_0^r+\omega)}{2})}{\cos(\omega_0^r+\omega)^2+\cos(\omega_0^i+\omega)^2}, \tag{B.7}$$

where V_1 represents a periodically oscillating function whose magnitude is no more than three. The magnitude of V_1 should be far less than $\frac{\omega\cos(\omega_{0p}^r+\omega_0^r+\omega)}{2}$ when ω is not too small.

$$\begin{aligned}V_1(\omega) :=&\frac{\sin(\omega_{0p}^r-\omega_0^r+\omega)}{4}+\frac{\sin(\omega_0^r-\omega_{0p}^r+\omega)}{4}-\frac{\sin(\omega_{0p}^i-\omega_0^i+\omega)}{4}-\\&\frac{\sin(\omega_0^i-\omega_{0p}^i+\omega)}{4}+\sin(\omega_0^i+\omega)-\sin(\omega_0^i)\end{aligned} \tag{B.8}$$

The same estimation could be performed on the other three terms of right-hand-side of Eq.(B.1), which all yield to similar result to above one. The calculation process hereby is skipped and the results are given directly:

$$\begin{aligned}&\frac{g_i(f_i*g_r+f_r*g_i)}{g_r^2-g_i^2}\\\approx&\frac{\alpha l}{\beta}\Phi_2(\omega),\quad l=(l_r+l_i)/2\end{aligned} \tag{B.9}$$

$$\begin{aligned}&\frac{g_i(f_i*g_i-f_r*g_r)}{g_r^2+g_i^2}\\\approx&\frac{\alpha l}{\beta}\Phi_3(\omega),\quad l=(l_r+l_i)/2\end{aligned} \tag{B.10}$$

$$\begin{aligned}&\frac{g_r(f_i*g_r+f_r*g_i)}{g_r^2+g_i^2}\\\approx&\frac{\alpha l}{\beta}\Phi_4(\omega),\quad l=(l_r+l_i)/2\end{aligned} \tag{B.11}$$

where $\Phi_i(\omega)$ could be approximated as follows if ω is not too small and $\xi \approx 1$:

$$\Phi_2(\omega) \approx \frac{-\cos(\omega_0^i+\omega)(V_2+\frac{\omega\cos(\omega_{0p}^i+\omega_0^r+\omega)}{2})}{\cos(\omega_0^r+\omega)^2+\cos(\omega_0^i+\omega)^2}, \tag{B.12}$$

$$\Phi_3(\omega) \approx \frac{-\cos(\omega_0^i+\omega)(V_3+\frac{\omega\cos(\omega_{0p}^r+\omega_0^r+\omega)}{2})}{\cos(\omega_0^r+\omega)^2+\cos(\omega_0^i+\omega)^2}, \tag{B.13}$$

$$\Phi_4(\omega) \approx \frac{\cos(\omega_0^r+\omega)(V_4+\frac{\omega\cos(\omega_{0p}^i+\omega_0^r+\omega)}{2})}{\cos(\omega_0^r+\omega)^2+\cos(\omega_0^i+\omega)^2}. \tag{B.14}$$

The expression of $V_i(i=2,3,4)$ is highly similar to V_1 and trivial thus would not be displayed.

Therefore,

$$\frac{\hat{P}_i(\omega)*\hat{e}_i^n(A)}{\hat{e}_i^n(A)} = \frac{\alpha l}{\beta}((\Phi_1+\Phi_2)+(\Phi_3+\Phi_4)j). \tag{B.15}$$